

Hierarchical Online Convex Optimization with Application to Multi-TRP Cooperative Networks

Juncheng Wang, *Student Member, IEEE*, Ben Liang, *Fellow, IEEE*, Min Dong, *Senior Member, IEEE*, Gary Boudreau, *Senior Member, IEEE*, and Hatem Abou-zeid, *Member, IEEE*

Abstract—We consider online convex optimization (OCO) over a heterogeneous network with communication delay, where multiple local devices (workers) together with a central coordinator (master) execute a sequence of decisions to minimize the accumulation of time-varying global costs. The local data may not be independent or identically distributed, and the global cost functions may not be locally separable. Due to communication delay, neither the master nor the workers have in-time information about the current global cost function. We propose a new algorithm, termed Hierarchical OCO (HiOCO), which takes full advantage of the network heterogeneity in information timeliness and computation capacity to enable multi-step gradient descent at both the workers and the master. We analyze the impacts of the unique hierarchical architecture, multi-slot delay, and gradient estimation error to derive upper bounds on the dynamic regret of HiOCO, which measures the gap of costs between HiOCO and an offline globally optimal performance benchmark. We further apply HiOCO to an online cooperative precoding design problem in multiple transmission/reception point (TRP) wireless networks with non-ideal backhaul links for 5G New Radio. Simulation results demonstrate substantial performance gain of HiOCO over existing alternatives.

Index Terms—Online convex optimization, master-worker network, non-separable cost, multi-TRP, cooperative precoding.

I. INTRODUCTION

Many machine learning, signal processing, and resource allocation problems can be cast into a dynamic optimization problem with time-varying convex cost functions. Online convex optimization (OCO) provides the tools to handle these dynamic problems in the presence of uncertainty, where an online decision strategy evolves based on the historical information [1]. OCO can be seen as a discrete-time sequential learning and decision-making process by an agent in a system. At the beginning of each time slot, the agent makes a decision from a convex feasible set. The system reveals information about the current convex cost function to the agent only at the end of each time slot. The lack of in-time information prevents the agent from making an optimal decision at each time slot. Instead, the agent resorts to minimizing the *regret*, which is the performance gap between the online decision sequence and some benchmark solution.

Most of the early works on OCO studied the *static regret*, which compares the online decision sequence with a static

offline benchmark [2]-[5]. However, the optimum of dynamic problems is often time varying. As a rather coarse performance metric, achieving sublinear static regret may not be meaningful since the static offline benchmark itself may perform poorly. The more attractive notion of *dynamic regret* was also proposed in [2], where the offline benchmark solution can be time varying. Dynamic regret bounds are often expressed in terms of certain variation measures that reflect how dynamic the system is. Theoretical guarantees on the dynamic regret for convex and strongly convex cost functions were studied in [2], [6]-[7] and [8]-[11], respectively.

The works [2]-[11] focused on centralized OCO, so they did not consider the network heterogeneity in information timeliness and computation capacity in many practical applications. For example, consider the multiple transmission/reception point (TRP) cooperative network in 5G New Radio (NR) [12]. Each TRP has more timely local channel state information (CSI) but less computation capacity compared with the central coordinator. In mobile edge computing [13], the local processors have timely information about their own computing tasks but may offload some tasks to the edge server due to the limitation on local computation resources. Another example is self-driving vehicular networks, where each vehicle moves based on its real-time sensor data while reporting local observations to a control center for traffic routing or utility maximization. In these examples, data are distributed away from the central coordinator and vary over time. Furthermore, the local devices need to make real-time decisions for global cost minimization. Applying centralized OCO approaches [2]-[11] to these systems would lead to degraded performance, since they do not fully utilize the computing capability or information timeliness of all network nodes.

Existing works on distributed OCO [14]-[23] are confined to *separable* global cost functions, *i.e.*, they can be expressed as a sum of local cost functions. Specifically, each local cost function depends only on the local data, which allows each node to locally compute the gradient of its own cost function without information about the data at the other nodes. However, in many practical systems, including the aforementioned joint multi-TRP transmission, mobile edge computing, and self-driving vehicular networks, the global cost functions are often *non-separable*, due to the coupling of data or decision variables at different nodes. For instance, in the multi-TRP cooperative precoding design example considered later in this paper, the transmissions of TRPs are coupled by the broadcast nature of the wireless channel. The solutions of [14]-[23] are not applicable to such systems.

J. Wang and B. Liang are with the University of Toronto (e-mail: {jcheng.wang, liang}@ece.utoronto.ca). M. Dong is with the Ontario Tech University (e-mail: min.dong@ontariotechu.ca). G. Boudreau and H. Abou-zeid are with Ericsson Canada (e-mail: {gary.boudreau, hatem.abou-zeid}@ericsson.com). This work has been funded in part by Ericsson Canada and by the Natural Sciences and Engineering Research Council (NSERC) of Canada.

Furthermore, in practical systems, the decision makers often gain access to the system information only after some delay. For example, in wireless networks, data transmission relies on the CSI, which is usually delayed for multiple transmission frames after channel acquisition and feedback. In the standard OCO setting, the decision maker receives information about the current cost function at the end of each time slot when the decision is made, *i.e.*, the feedback information is delayed for only one time slot. This is the setting used in all existing distributed OCO works [14]-[23], but it can be too restrictive for many practical applications.

In this work, we aim to develop an online learning algorithm that takes full advantage of the network heterogeneity in information timeliness and computation capacity, while allowing the global cost functions to be non-separable and accommodating multi-slot information delay. The main contributions of this paper are as follows:

- We formulate a new OCO problem for a heterogeneous master-worker network with communication delay, where the worker nodes have timely information about the local data but possibly less computation resources compared with the master node. At the beginning of each time slot, each worker node executes a local decision to minimize the accumulation of time-varying global costs. The local data at the worker nodes may not be independent or identically distributed, the global cost functions may be non-separable, and the feedback and data acquisition delay may span multiple time slots. This new problem formulation has many practical applications and broadens the scope of OCO in the existing literature.
- We propose a new Hierarchical Online Convex Optimization (HiOCO) algorithm that takes full advantage of the network heterogeneity in information timeliness and computation capacity. HiOCO allows both *timely local* gradient descent at the worker nodes and *delayed global* gradient descent at the master node to improve system performance. Furthermore, HiOCO allows multi-step estimated gradient descent at both the worker nodes and the master node to fully utilize their computation resources.
- We analyze the special structure of HiOCO in terms of its hierarchical multi-step estimated gradient descent, in the presence of multi-slot delay. We prove that it yields $\mathcal{O}(\min\{\max\{\tau\Pi_T^*, \Delta_T\}, \max\{\tau^2\Pi_{2,T}^*, \Delta_{2,T}\}\})$ dynamic regret, where τ is the total feedback delay, and Π_T^* , $\Pi_{2,T}^*$, Δ_T , and $\Delta_{2,T}$ are certain variation measures that represent how dynamic the system is (see definitions in Section III-C). We further extend our analysis to the case where even the worker nodes experience multi-slot delay to collect their local data.
- We apply HiOCO to an online multi-TRP cooperative precoding design problem. Simulation under typical urban micro-cell Long-Term Evolution (LTE) settings demonstrates that, by carefully combining both local and central estimated gradient descent with different levels of information delay, HiOCO can substantially improve system performance, outperforming existing alternatives.

Organization: The rest of this paper is organized as follows. In Section II, we present the related work. Section III describes the system model, problem formulation, and performance metrics for OCO. We present the HiOCO algorithm, prove its dynamic regret bounds, and discuss its performance merits in Section IV. We further extend HiOCO to the case of non-zero local delay in Section V. The application of HiOCO to an online multi-TRP cooperative precoding design problem is presented in Section VI. Simulation results are provided in Section VII, followed by concluding remarks in Section VIII.

Notations: Scalars are denoted by letters in regular font, while vectors (resp. matrices) are denoted by bold face (resp. capital) letters. The transpose, complex conjugate, Hermitian transpose, L_2 norm, L_∞ norm, Frobenius norm, and the (i, j) element of a matrix \mathbf{A} are denoted by \mathbf{A}^T , \mathbf{A}^* , \mathbf{A}^H , $\|\mathbf{A}\|$, $\|\mathbf{A}\|_\infty$, $\|\mathbf{A}\|_F$, and $[\mathbf{A}]_{i,j}$, respectively. The notation $\mathbb{E}\{\cdot\}$ denotes expectation, $\langle \mathbf{a}, \mathbf{b} \rangle$ denotes the Euclidean inner product of vectors \mathbf{a} and \mathbf{b} , and $\mathbf{g} \sim \mathcal{CN}(\mathbf{0}, \sigma^2 \mathbf{I})$ means that \mathbf{g} is a circular complex Gaussian random vector with mean $\mathbf{0}$ and variance $\sigma^2 \mathbf{I}$, where \mathbf{I} represents the identity matrix.

II. RELATED WORK

In this section, we survey existing works on OCO.¹ The differences between the existing literature and our work are summarized in Table I.

A. Online Learning and OCO

Online learning is a method of machine learning where a learner attempts to tackle some decision-making task by learning from a sequence of data instances. As an important subclass of online learning, OCO has been applied in various areas such as wireless communications, cloud networks, and smart grids.

In the seminal work of OCO [2], an online projected gradient descent algorithm achieves $\mathcal{O}(\sqrt{T})$ static regret with bounded feasible set and gradient, where T is the time horizon. The static regret was shown to be unavoidably $\Omega(\sqrt{T})$ for general convex cost functions without additional assumptions, but it was further improved to $\mathcal{O}(\log T)$ for strongly convex cost functions [3]. In the standard OCO setting, information feedback is delayed for only one time slot, which is restrictive for many practical applications. The standard online projected gradient descent algorithm was extended in [4] to provide $\mathcal{O}(\sqrt{\tau T})$ static regret in the presence of τ -slot delay. Moreover, [5] studied OCO with adversarial delay.

The dynamic regret of OCO was first introduced in [2], and it has received a recent surge of interest [6], [7]. Strong convexity was shown to improve the dynamic regret bound in [8]. By increasing the number of gradient descent steps, the dynamic regret bound was further improved in [9]. Furthermore, extensions to accommodate inexact gradient were proposed in [10] and [11] with dynamic regret analysis.

Centralized OCO algorithms [2]-[11] naturally do not require the global cost function to be separable. Therefore, they

¹We focus on common short-term constrained OCO. OCO with long-term constraints are out of the scope of this paper. We refer interested readers to [24]-[26] and references therein.

TABLE I
SUMMARY OF RELATED DYNAMIC REGRET BOUNDS FOR OCO

References	Gradient calculation	Cost function	Non-separable cost	Inaccurate gradient	Feedback delay	Dynamic regret (see definitions in Section III-C)
[2]	Central	Convex	Allowed	Not allowed	$\tau = 1$	$\mathcal{O}(\Pi_T \sqrt{T})$
[7]	Central	Convex	Allowed	Not allowed	$\tau = 1$	$\mathcal{O}(\min\{\sqrt{\Gamma_{2,T}\Pi_T^*}, (\Gamma_{2,T}\Theta_T T)^{\frac{1}{3}}\})$
[8]	Central	Strongly convex	Allowed	Not allowed	$\tau = 1$	$\mathcal{O}(\Pi_T^*)$
[9]	Central	Strongly Convex	Allowed	Not allowed	$\tau = 1$	$\mathcal{O}(\min\{\Pi_T^*, \Pi_{2,T}^*\})$
[10], [11]	Central	Strongly Convex	Allowed	Allowed	$\tau = 1$	$\mathcal{O}(\max\{\Pi_T^*, \Delta_T\})$
[21], [22]	Local	Convex	Not allowed	Not allowed	$\tau = 1$	$\mathcal{O}(\sqrt{\Pi_T^* T})$
[23]	Local	Strongly Convex	Not allowed	Not allowed	$\tau = 1$	$\mathcal{O}(\max\{\Pi_T^*, \Gamma_T\})$
HiOCO	Local and Central	Strongly Convex	Allowed	Allowed	$\tau \geq 1$	$\mathcal{O}(\min\{\max\{\tau\Pi_T^*, \Delta_T\}, \max\{\tau^2\Pi_{2,T}^*, \Delta_{2,T}\}\})$

can be applied to the online optimization problem we consider in this work. However, this way of solving the problem does not utilize the information timeliness or computation capacity at all network nodes. This can lead to substantial degradation of system performance compared with the proposed HiOCO approach, as demonstrated in Section VII.

B. Distributed OCO

Early works on distributed OCO focused on the static regret [14]-[20]. A distributed online algorithm based on dual averaging was proposed in [14]. It achieves $\mathcal{O}(\sqrt{T})$ static regret. Another dual averaging based algorithm was shown to yield $\mathcal{O}(\log T)$ static regret for strongly convex cost functions [15]. Further extensions include Nesterov's primal-dual approach [16] and approximate dual averaging [17]. Any-batch dual averaging was proposed in [18]. The impact of network topology on the performance of distributed OCO was studied in [19] and [20].

More recent works on distributed OCO considered the dynamic regret, since it is a better measurement of performance when the system environment is time-varying. Distributed mirror descent for online optimization was studied in [21]. Any-batch mirror descent was proposed in [22] for heterogeneous networks. In [23], a push-pull based online algorithm provided an improved dynamic regret for strongly convex cost functions.

Existing works on distributed OCO are confined to separable global cost functions. For non-separable global cost minimization in distributed networks, more information exchange is needed among the network nodes. Furthermore, these works are under the standard OCO setting with one-slot feedback delay. In contrast, HiOCO accommodates both non-separable global cost functions and multi-slot feedback delay, in a heterogeneous master-worker network.

III. SYSTEM MODEL AND PROBLEM FORMULATION

A. System Model

We consider OCO over a master-worker network in a time-slotted system with time indexed by t . Since we are interested in non-separable global cost functions, it is imperative to have a master node that can collect certain global information from distributed data. Among the examples given in Section I, the master node can be the central coordinator in a multi-TRP cooperative network, the edge server in a mobile edge computing network, or the central controller at a nearby Road Side Unit in a vehicular network.

As shown in Fig. 1, the master node is connected to C worker nodes through separate communication links. Denote by τ_r^u the *remote uplink* delay for the worker nodes to upload information to the master node, and by τ_r^d the *remote downlink* delay for the master node to send information back to the worker nodes. Further denote the remote round-trip delay between the master node and the worker nodes by $\tau_r = \tau_r^u + \tau_r^d$.² In the standard OCO setting, information feedback is assumed to be delayed for only one time slot. However, in many practical applications such as those mentioned in Section I, this assumption is rarely satisfied since information can be severely delayed. Therefore, in this work, we consider multi-slot delay, *i.e.*, $\tau_r \geq 1$.

We also consider local delay denoted by τ_l for the worker nodes to collect their own data. For example, in the multi-TRP joint transmission problem considered later in this work, local CSI may be delayed at the TRPs. For ease of exposition, we will first consider the case $\tau_l = 0$. Then, in Section V, we will discuss the case $\tau_l > 0$.

At the beginning of each time slot t , each worker node c collects some local data \mathbf{d}_t^c . In a large distributed network, the local data at each node often cannot be regarded as samples drawn from the same overall distribution. Furthermore, the underlying system is often time-varying in many practical applications. Therefore, we allow $\{\mathbf{d}_t^c\}_{c=1}^C$ to be non-independent and non-identically distributed and to vary arbitrarily over time with unknown statistics.

B. Problem Formulation

Let $f(\{\mathbf{d}_t^c\}_{c=1}^C, \{\mathbf{x}_t^c\}_{c=1}^C) : \mathbb{R}^n \rightarrow \mathbb{R}$ be the *global* convex cost function at time slot t , where \mathbf{x}^c is a local decision vector at worker node c , which has dimension n^c . We consider constraints represented by a compact convex set $\mathcal{X}^c \in \mathbb{R}^{n^c}$ at each worker node c . The worker nodes and the master node cooperate to jointly select a sequence of decisions $\{\{\mathbf{x}_t^c\}_{c=1}^C\}_{t=1}^T$ from the feasible sets that minimizes the accumulated time-varying global costs. This leads to the following optimization problem:

$$\mathbf{P1} : \min_{\{\{\mathbf{x}_t^c \in \mathcal{X}^c\}_{c=1}^C\}_{t=1}^T} \sum_{t=1}^T f(\{\mathbf{d}_t^c\}_{c=1}^C, \{\mathbf{x}_t^c\}_{c=1}^C).$$

Existing distributed gradient descent algorithms implicitly assume each node c can locally compute its own gradient

²We show later in Section IV-A that only the round-trip delay impacts the online decision-making process.

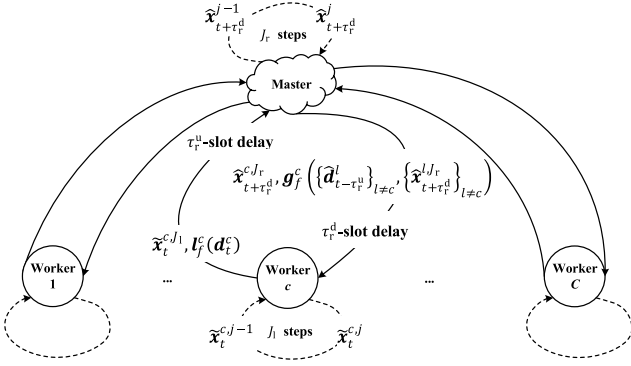


Fig. 1. OCO over a master-worker network with communication delay (showing the case of zero local delay for illustration).

$\nabla_{\mathbf{x}^c} f(\{\mathbf{d}_t^c\}_{c=1}^C, \{\mathbf{x}^c\}_{c=1}^C)$ based only on the local information [14]-[23]. These algorithms focus on separable global cost functions, *i.e.*, $f(\{\mathbf{d}_t^c\}_{c=1}^C, \{\mathbf{x}^c\}_{c=1}^C)$ can be expressed as a summation of C local cost functions, each corresponding only to the local data \mathbf{d}_t^c and decision vector \mathbf{x}^c .³ In this work, we consider the general case where the global cost functions may be *non-separable* among the worker nodes. Therefore, due to the coupling of data or variables, each worker node c cannot locally compute its own gradient without information exchange with the other nodes.

For non-separable global cost functions, the local gradient at each worker node c may depend on its local data \mathbf{d}_t^c , local decision vector \mathbf{x}^c , and possibly the data \mathbf{d}_t^l and decision vector \mathbf{x}^l at any other worker node $l \neq c$. Therefore, we define the local gradient at each worker node c as a general function denoted by $\mathbf{h}_f^c(\cdot)$ as follows:

$$\begin{aligned} \nabla_{\mathbf{x}^c} f(\{\mathbf{d}_t^c\}_{c=1}^C, \{\mathbf{x}^c\}_{c=1}^C) \\ \triangleq \mathbf{h}_f^c(\mathbf{d}_t^c, \mathbf{x}^c, \mathbf{g}_f^c(\{\mathbf{d}_t^l\}_{l \neq c}, \{\mathbf{x}^l\}_{l \neq c})) \end{aligned} \quad (1)$$

where $\mathbf{g}_f^c(\cdot)$ is some global information function. Note that $\mathbf{h}_f^c(\cdot)$ and $\mathbf{g}_f^c(\cdot)$ depend on the specific format of $f(\cdot)$. We will show using an example later in Section VI that, communicating the values of $\mathbf{g}_f^c(\cdot)$ can often reduce the communication overhead compared with sending the variables $\{\mathbf{d}_t^l\}_{l \neq c}$ and $\{\mathbf{x}^l\}_{l \neq c}$ directly.

C. Performance Metric and Measure of Variation

For notation simplicity, in the following, we define the global feasible set as $\mathcal{X} \triangleq \cup_{c=1}^C \{\mathcal{X}^c\} \in \mathbb{R}^n$ and denote the global cost function by

$$f_t(\mathbf{x}) \triangleq f(\{\mathbf{d}_t^c\}_{c=1}^C, \{\mathbf{x}^c\}_{c=1}^C)$$

where $\mathbf{x} \triangleq [\mathbf{x}^1, \dots, \mathbf{x}^C]^T \in \mathbb{R}^n$ is the global decision vector. In addition, the local gradient $\nabla_{\mathbf{x}^c} f(\{\mathbf{d}_t^c\}_{c=1}^C, \{\mathbf{x}^c\}_{c=1}^C)$ at each worker node c is denoted by $\nabla f_t^c(\mathbf{x}^c)$.

Due to the lack of in-time information about the global cost function at either the worker nodes or the master node, it is impossible to obtain an optimal solution to $\mathbf{P1}$.⁴ Instead,

³Specifically, [14]-[23] assumes $f(\{\mathbf{d}_t^c\}_{c=1}^C, \mathbf{w}) = \sum_{c=1}^C f(\mathbf{d}_t^c, \mathbf{w})$, where \mathbf{w} is a global decision vector. It is a special case of our global cost function $f(\{\mathbf{d}_t^c\}_{c=1}^C, \{\mathbf{x}^c\}_{c=1}^C)$ by letting $\mathbf{x}^c = \mathbf{w}$ for any $c \in \{1, \dots, C\}$.

⁴In fact, even for the most basic centralized OCO problem [2], an optimal solution cannot be found [3].

we aim at selecting an online solution sequence $\{\mathbf{x}_t\}_{t=1}^T$ that keeps tracking the optimal dynamic solution sequence $\{\mathbf{x}_t^*\}_{t=1}^T$, given by

$$\mathbf{x}_t^* \in \arg \min_{\mathbf{x} \in \mathcal{X}} \{f_t(\mathbf{x})\}. \quad (2)$$

Note that \mathbf{x}_t^* is computed with the current information about $f_t(\mathbf{x})$. The corresponding dynamic regret is defined as

$$\text{RE}_T^d \triangleq \sum_{t=1}^T (f_t(\mathbf{x}_t) - f_t(\mathbf{x}_t^*)), \quad (3)$$

which is commonly adopted in the existing literature, *e.g.*, [7]-[11], [21]-[23]. The dynamic regret can be bounded in terms of different variation measures that represent how dynamic the system is and hence the hardness of the problem. We introduce several common variation measures as follows.

The path-length of an arbitrary sequence of reference points $\{\mathbf{r}_t \in \mathcal{X}\}_{t=1}^T$ is defined as $\Pi_T \triangleq \sum_{t=1}^T \|\mathbf{r}_t - \mathbf{r}_{t-1}\|$ [2]. The online projected gradient descent algorithm in [2] achieves $\mathcal{O}(\Pi_T \sqrt{T})$ dynamic regret with respect to (w.r.t.) $\{\mathbf{r}_t\}_{t=1}^T$. When the reference points are the per-slot optimal solutions, *i.e.*, $\mathbf{r}_t = \mathbf{x}_t^*$ for all t , the resulting path-length is

$$\Pi_T^* \triangleq \sum_{t=1}^T \|\mathbf{x}_t^* - \mathbf{x}_{t-1}^*\|. \quad (4)$$

For example, the optimistic mirror descent algorithm in [7] achieves $\mathcal{O}(\min\{\sqrt{\Gamma_{2,T} \Pi_T^*}, (\Gamma_{2,T} \Theta_T T)^{\frac{1}{3}}\})$ dynamic regret, where $\Theta_T \triangleq \sum_{t=1}^T \max_{\mathbf{x} \in \mathcal{X}} \{f_t(\mathbf{x}) - f_{t-1}(\mathbf{x})\}$ and $\Gamma_{2,T} \triangleq \sum_{t=1}^T \|\nabla f_t(\mathbf{x}_t) - \nabla f_{t-1}(\mathbf{x}_{t-1})\|^2$. As another example, when the cost functions are strongly convex, the one-step gradient descent algorithm in [8] achieves $\mathcal{O}(\Pi_T^*)$ dynamic regret.

Another important variation measure is the squared path-length, defined as

$$\Pi_{2,T}^* \triangleq \sum_{t=1}^T \|\mathbf{x}_t^* - \mathbf{x}_{t-1}^*\|^2. \quad (5)$$

For example, the multi-step gradient descent algorithm in [9] improves the dynamic regret to $\mathcal{O}(\min\{\Pi_T^*, \Pi_{2,T}^*\})$ for strongly convex cost functions. Note that $\Pi_{2,T}^*$ is often smaller than Π_T^* in the order sense [9].⁵

Further variation measures are required when we use inexact gradients. For example, the standard and proximal online gradient descent algorithms were respectively extended in [10] and [11] to accommodate inexact gradients. Both achieve $\mathcal{O}(\max\{\Pi_T^*, \Delta_T\})$ dynamic regret, where Δ_T is the accumulated gradient error defined as

$$\Delta_T \triangleq \sum_{t=1}^T \max_{\mathbf{x} \in \mathcal{X}} \|\nabla f_t(\mathbf{x}) - \nabla \hat{f}_t(\mathbf{x})\| \quad (6)$$

where $\nabla \hat{f}_t(\cdot)$ is a given function available at the decision maker to predict the current gradient.

⁵For instance $\|\mathbf{x}_t^* - \mathbf{x}_{t-1}^*\| \propto T^\rho$ for any t , then $\Pi_T^* = \mathcal{O}(T^{1+\rho})$ and $\Pi_{2,T}^* = \mathcal{O}(T^{1+2\rho})$. For a sublinear Π_T^* or $\Pi_{2,T}^*$, we have $\rho < 0$ and therefore $\Pi_{2,T}^*$ is smaller than Π_T^* in the order sense. Particularly, if $\rho = -\frac{1}{2}$, we have $\Pi_{2,T}^* = \mathcal{O}(1)$ and $\Pi_T^* = T^{\frac{1}{2}}$.

For the performance bounding of HiOCO in Section IV-B, we further define the accumulated squared gradient error as

$$\Delta_{2,T} \triangleq \sum_{t=1}^T \max_{\mathbf{x} \in \mathcal{X}} \{ \|\nabla f_t(\mathbf{x}) - \nabla \hat{f}_t(\mathbf{x})\|^2 \}. \quad (7)$$

Similar to the relationship between $\Pi_{2,T}^*$ and Π_T^* , $\Delta_{2,T}$ is often smaller than Δ_T in the order sense.

The above works [2], [7]-[11] focus on centralized OCO. For distributed OCO, the mirror descent algorithm in [21] achieves $\mathcal{O}(\sqrt{\Pi_T^* T})$ dynamic regret. The any-bach mirror descent algorithm in [22] accommodates time-varying batch sizes while recovering the dynamic regret in [21] as a special case. The impact of strongly convex cost functions on the dynamic regret of distributed OCO has been considered in [23]. The push-pull based online algorithm provides $\mathcal{O}(\Pi_T^*, \Gamma_T)$ dynamic regret, where $\Gamma_T \triangleq \sum_{t=1}^T \|\nabla f_t(\mathbf{x}_t) - \nabla f_{t-1}(\mathbf{x}_{t-1})\|_\infty$. In this work, we will derive dynamic regret bounds using variation measures defined in (4)-(7).

IV. HIERARCHICAL ONLINE CONVEX OPTIMIZATION

In this section, we first present the design details of HiOCO. We then study the impact of hierarchical multi-step estimated gradient descent on the performance of HiOCO in terms of its dynamic regret. We further give sufficient conditions under which HiOCO yields sublinear dynamic regret. Finally, we discuss the performance merits of HiOCO over existing OCO algorithms in terms of the dynamic regret bound.

A. HiOCO Algorithm Description

Existing distributed OCO algorithms [14]-[23] cannot be directly applied to solve **P1** with non-separable global cost functions. As an alternative, one may apply centralized OCO [2]-[11] at the master node after it has received all the local data from the worker nodes. However, this way of solving the problem does not take advantage of the more timely local information at the worker nodes, nor their computation resources.

Different from existing centralized and distributed OCO algorithms, in HiOCO, the master node and the worker nodes cooperate in gradient estimation and decision updates, by taking full advantage of the network heterogeneity in information timeliness and computation capacity. For ease of exposition, we first consider the case of zero local delay at the worker nodes but will extend that to the case of non-zero local delay in Section V. In the following, we present HiOCO algorithms at the master node and the worker nodes.

1) *Master Node's Algorithm:* In practical systems, the master node often has a higher computation capacity compared with the worker nodes. To leverage this capacity, we design HiOCO to be capable of performing central gradient descent at the master node. In this case, each worker node c needs to share information about its local data \mathbf{d}_t^c with the master node. Each worker node c sends a compressed version of the current local data $\mathbf{I}_f^c(\mathbf{d}_t^c)$ to the master node, where $\mathbf{I}_f^c(\cdot)$ is some general function for data compression. Note that the need for information exchange about the local data is

unavoidable in order to optimize non-separable global cost functions, regardless whether a master node is used.

At the beginning of each time slot t , each worker node c executes its current local decision vector \mathbf{x}_t^c and then uploads it together with $\mathbf{I}_f^c(\mathbf{d}_t^c)$ to the master node. Due to the remote uplink delay, at the beginning of each time slot t , the master node only has the τ_r^u -slot-delayed local decision vector $\mathbf{x}_{t-\tau_r^u}^c$ and compressed data $\mathbf{I}_f^c(\mathbf{d}_{t-\tau_r^u}^c)$ from each worker node c . The master node then recovers an estimated version of the local data $\hat{\mathbf{d}}_{t-\tau_r^u}^c$ from $\mathbf{I}_f^c(\mathbf{d}_{t-\tau_r^u}^c)$, which is then used to generate new decision vectors to assist the local decision-making processes at the worker nodes.⁶

Note that the master node needs to consider the remote downlink delay and design the decision vectors for the worker nodes τ_r^d -slot ahead based on the τ_r^u -slot delayed information. One can easily verify that only the round-trip remote delay τ_r impacts the decision-making process. Therefore, in the following, without loss of generality, we only need to consider the case of τ_r -slot remote uplink delay and zero remote downlink delay.

Remark 1. There is often a delay-accuracy tradeoff for the recovered data $\{\hat{\mathbf{d}}_{t-\tau_r}^c\}_{c=1}^C$ at the master node, since a higher data compression rate reduces the data transmission time but also reduces the data accuracy at the master node. If data privacy is a concern, the worker nodes can also add noise to the compressed data while sacrificing some system performance [27].

With $\{\mathbf{x}_{t-\tau_r}^c\}_{c=1}^C$ and $\{\hat{\mathbf{d}}_{t-\tau_r}^c\}_{c=1}^C$, for each worker node c , the master node sets an intermediate decision vector $\hat{\mathbf{x}}_t^{c,0} = \mathbf{x}_{t-\tau_r}^c$ and performs J_r -step gradient descent to generate $\hat{\mathbf{x}}_t^{c,J_r}$.⁷ For each gradient descent step $j \in \{1, \dots, J_r\}$, the master node solves the following optimization problem for $\hat{\mathbf{x}}_t^{c,j}$:

$$\mathbf{P2} : \min_{\mathbf{x}^c \in \mathcal{X}^c} \langle \nabla \hat{f}_{t-\tau_r}^c(\hat{\mathbf{x}}_t^{c,j-1}), \mathbf{x}^c - \hat{\mathbf{x}}_t^{c,j-1} \rangle + \frac{\alpha}{2} \|\mathbf{x}^c - \hat{\mathbf{x}}_t^{c,j-1}\|^2$$

where $\nabla \hat{f}_{t-\tau_r}^c(\hat{\mathbf{x}}_t^{c,j-1})$ is an *estimated* gradient based on the delayed global information $\{\hat{\mathbf{d}}_{t-\tau_r}^c\}_{c=1}^C$, and it is given by

$$\begin{aligned} & \nabla \hat{f}_{t-\tau_r}^c(\hat{\mathbf{x}}_t^{c,j-1}) \\ & \triangleq \mathbf{h}_f^c \left(\hat{\mathbf{d}}_{t-\tau_r}^c, \hat{\mathbf{x}}_t^{c,j-1}, \mathbf{g}_f^c \left(\{\hat{\mathbf{d}}_{t-\tau_r}^l\}_{l \neq c}, \{\hat{\mathbf{x}}_t^{l,j-1}\}_{l \neq c} \right) \right). \end{aligned} \quad (8)$$

The master node then sends $\hat{\mathbf{x}}_t^{c,J_r}$ and the corresponding global information $\mathbf{g}_f^c(\{\hat{\mathbf{d}}_{t-\tau_r}^l\}_{l \neq c}, \{\hat{\mathbf{x}}_t^{l,J_r}\}_{l \neq c})$ to assist the local decision-making process at each worker node c . In Algorithm 1, we summarize the master node's algorithm.

Remark 2. Note that even though the master node has global information about the data, this information is delayed and inexact. In HiOCO, different from the centralized approaches [2]-[11], the central decisions made at the master node are not used directly as the final solution, but are used later at the worker nodes to assist their local decision-making processes.

⁶The compression and recovery techniques on the data can be chosen based on specific applications and are beyond the scope of this paper.

⁷Later in Sections IV-B and VII, we show that multi-step gradient descent in HiOCO improves the dynamic regret bound and system performance.

Algorithm 1 HiOCO master node's algorithm

- 1: Initialize $\alpha > 0$ and broadcast it to each worker node c .
- 2: At the beginning of each $t > \tau_r$, do the following:
- 3: Receive $\mathbf{x}_{t-\tau_r}^c$ and $\mathbf{l}_f^c(\mathbf{d}_{t-\tau_r}^c)$ from each worker node c .
- 4: Estimate $\hat{\mathbf{d}}_{t-\tau_r}^c$ from $\mathbf{l}_f^c(\mathbf{d}_{t-\tau_r}^c)$.
- 5: Set $\hat{\mathbf{x}}_t^{c,0} = \mathbf{x}_{t-\tau_r}^c$ for each worker node c .
- 6: **for** $j = 1$ **to** J_r
- 7: Construct estimated gradient $\nabla \hat{f}_{t-\tau_r}^c(\hat{\mathbf{x}}_t^{c,j-1})$ in (8).
- 8: Update $\hat{\mathbf{x}}_t^{c,j}$ for each worker node c by solving **P2**.
- 9: **end for**
- 10: Send $\hat{\mathbf{x}}_t^{c,J_r}$ and $\mathbf{g}_f^c(\{\hat{\mathbf{d}}_{t-\tau_r}^l\}_{l \neq c}, \{\hat{\mathbf{x}}_t^{l,J_r}\}_{l \neq c})$ to each worker node c .

2) *Worker Node c 's Algorithm:* The worker nodes have the most up-to-date information about their own local data. However, when the global cost function is non-separable, each worker node c cannot compute its own gradient $\nabla f_t^c(\mathbf{x}_t^c) = \mathbf{h}_f^c(\mathbf{d}_t^c, \mathbf{x}_t^c, \mathbf{g}_f^c(\{\mathbf{d}_t^l\}_{l \neq c}, \{\mathbf{x}_t^l\}_{l \neq c}))$ based only on the local information. Therefore, in HiOCO, the master node assists the local gradient estimation by communicating the required global information $\mathbf{g}_f^c(\{\hat{\mathbf{d}}_{t-\tau_r}^l\}_{l \neq c}, \{\hat{\mathbf{x}}_t^{l,J_r}\}_{l \neq c})$ to each worker node c . Note that due to the communication delay and data compression, such global information received by each worker node c is delayed and inexact.

At the beginning of each time slot t , each worker node c receives the global information $\mathbf{g}_f^c(\{\hat{\mathbf{d}}_{t-\tau_r}^l\}_{l \neq c}, \{\hat{\mathbf{x}}_t^{l,J_r}\}_{l \neq c})$ together with the intermediate decision vector $\hat{\mathbf{x}}_t^{c,J_r}$ from the master node. Each worker node c then initializes another intermediate decision vector $\tilde{\mathbf{x}}_t^{c,0} = \hat{\mathbf{x}}_t^{c,J_r}$ and performs J_1 -step local gradient descent to generate $\tilde{\mathbf{x}}_t^{c,J_1}$. For each gradient descent step $j \in \{1, \dots, J_1\}$, each worker node c solves the following optimization problem for $\tilde{\mathbf{x}}_t^{c,j}$:

$$\mathbf{P3}: \min_{\mathbf{x}^c \in \mathcal{X}^c} \langle \nabla \hat{f}_t^c(\tilde{\mathbf{x}}_t^{c,j-1}), \mathbf{x}^c - \tilde{\mathbf{x}}_t^{c,j-1} \rangle + \frac{\alpha}{2} \|\mathbf{x}^c - \tilde{\mathbf{x}}_t^{c,j-1}\|^2$$

where $\nabla \hat{f}_t^c(\tilde{\mathbf{x}}_t^{c,j-1})$ is an *estimated* gradient based on the timely local data \mathbf{d}_t^c and the delayed global information $\mathbf{g}_f^c(\{\hat{\mathbf{d}}_{t-\tau_r}^l\}_{l \neq c}, \{\hat{\mathbf{x}}_t^{l,J_r}\}_{l \neq c})$, and it is given by

$$\begin{aligned} & \nabla \hat{f}_t^c(\tilde{\mathbf{x}}_t^{c,j-1}) \\ & \triangleq \mathbf{h}_f^c \left(\mathbf{d}_t^c, \tilde{\mathbf{x}}_t^{c,j-1}, \mathbf{g}_f^c \left(\{\hat{\mathbf{d}}_{t-\tau_r}^l\}_{l \neq c}, \{\hat{\mathbf{x}}_t^{l,J_r}\}_{l \neq c} \right) \right). \end{aligned} \quad (9)$$

The above estimated gradient takes full advantage of the information timeliness at the worker nodes, as well as the central availability of information at the master node, to enable local gradient descent at the worker nodes for non-separable global cost minimization. Each worker node c executes $\mathbf{x}_t^c = \tilde{\mathbf{x}}_t^{c,J_1}$ as its current local decision vector. It then uploads \mathbf{x}_t^c and the compressed local data $\mathbf{l}_f^c(\mathbf{d}_t^c)$ to the master node. In Algorithm 2, we summarize the worker node's algorithm.

Remark 3. The solutions to **P2** and **P3** are projected gradient descent updates. For example, solving **P2** for $\hat{\mathbf{x}}_t^{c,j}$ is equivalent to updating $\hat{\mathbf{x}}_t^{c,j}$ through

$$\hat{\mathbf{x}}_t^{c,j} = \mathcal{P}_{\mathcal{X}^c} \left\{ \hat{\mathbf{x}}_t^{c,j-1} - \frac{1}{\alpha} \nabla \hat{f}_{t-\tau_r}^c(\hat{\mathbf{x}}_t^{c,j-1}) \right\}$$

Algorithm 2 HiOCO worker node c 's algorithm

- 1: Initialize $\mathbf{x}_t^c \in \mathcal{X}^c$ at random for any $t \leq \tau_r$.
- 2: At the beginning of each $t > \tau_r$, do the following:
- 3: Receive $\hat{\mathbf{x}}_t^{c,J_r}$ and $\mathbf{g}_f^c(\{\hat{\mathbf{d}}_{t-\tau_r}^l\}_{l \neq c}, \{\hat{\mathbf{x}}_t^{l,J_r}\}_{l \neq c})$ from the master node.
- 4: Set $\tilde{\mathbf{x}}_t^{c,0} = \hat{\mathbf{x}}_t^{c,J_r}$.
- 5: **for** $j = 1$ **to** J_1
- 6: Construct estimated gradient $\nabla \hat{f}_t^c(\tilde{\mathbf{x}}_t^{c,j-1})$ in (9).
- 7: Update $\tilde{\mathbf{x}}_t^{c,j}$ by solving **P3**.
- 8: **end for**
- 9: Set $\mathbf{x}_t^c = \tilde{\mathbf{x}}_t^{c,J_1}$ and execute \mathbf{x}_t^c .
- 10: Send \mathbf{x}_t^c and $\mathbf{l}_f^c(\mathbf{d}_t^c)$ to the master node.

where $\mathcal{P}_{\mathcal{X}^c}\{\mathbf{x}^c\} \triangleq \arg \min_{\mathbf{y}^c \in \mathcal{X}^c} \{\|\mathbf{y}^c - \mathbf{x}^c\|^2\}$ is the projection operator onto the convex feasible set \mathcal{X}^c and α can be seen as a step-size parameter. We use **P2** and **P3** here for the ease of dynamic regret analysis later.

Remark 4. For separable global cost functions, HiOCO can still be applied. In this case, it is still beneficial to perform central gradient descent for improved system performance, while incurring some communication overhead caused by uploading the compressed local data.

Remark 5. Single-step and multi-step gradient descent algorithms were provided in [8] and [9], while [10] and [11] proposed single-step inexact gradient descent algorithms. All of these algorithms are centralized and are under the standard OCO setting with one-slot delay. In HiOCO, both the master node and the worker nodes can perform multi-step gradient descent with estimated gradients under multi-slot delay.

B. Dynamic Regret Bounds

In this section, we derive upper bounds on the dynamic regret of HiOCO. We develop new analysis techniques to account for its hierarchical multi-step gradient descent with estimated gradients, in the presence of multi-slot delay.

We focus on strongly convex functions, which arise in many machine learning and signal processing applications, such as Lasso regression, support vector machine, softmax classifier, and robust subspace tracking. Furthermore, for applications with general convex cost functions, it is common to add a simple regularization term such as $\frac{\mu}{2} \|\mathbf{x}\|^2$, so that the overall optimization objective becomes strongly convex [11]. We make the following assumptions that are common in the literature of OCO with strongly convex functions [8]-[11], [23].

Assumption 1. For any t , $f_t(\mathbf{x})$ satisfies the following:

- 1.1) $f_t(\mathbf{x})$ is μ -strongly convex over \mathcal{X} , i.e., $\exists \mu > 0$, s.t., for any $\mathbf{x}, \mathbf{y} \in \mathcal{X}$ and t

$$f_t(\mathbf{y}) \geq f_t(\mathbf{x}) + \langle \nabla f_t(\mathbf{x}), \mathbf{y} - \mathbf{x} \rangle + \frac{\mu}{2} \|\mathbf{y} - \mathbf{x}\|^2. \quad (10)$$

- 1.2) $f_t(\mathbf{x})$ is L -smooth over \mathcal{X} , i.e., $\exists L > 0$, s.t., for any $\mathbf{x}, \mathbf{y} \in \mathcal{X}$ and t

$$f_t(\mathbf{y}) \leq f_t(\mathbf{x}) + \langle \nabla f_t(\mathbf{x}), \mathbf{y} - \mathbf{x} \rangle + \frac{L}{2} \|\mathbf{y} - \mathbf{x}\|^2. \quad (11)$$

1.3) The gradient of $f_t(\mathbf{x})$ is bounded, i.e., $\exists D > 0$, s.t., for any $\mathbf{x} \in \mathcal{X}$ and t

$$\|\nabla f_t(\mathbf{x})\| \leq D. \quad (12)$$

Assumption 2. The radius of \mathcal{X} is bounded, i.e., $\exists R > 0$, s.t., for any $\mathbf{x}, \mathbf{y} \in \mathcal{X}$

$$\|\mathbf{x} - \mathbf{y}\| \leq R. \quad (13)$$

We require the following lemma, which is reproduced from Lemma 2.8 in [1].

Lemma 1. Let $\mathcal{X} \in \mathbb{R}^n$ be a nonempty convex set. Let $f(\mathbf{x}) : \mathbb{R}^n \rightarrow \mathbb{R}$ be a μ -strongly-convex function over \mathcal{X} . Let $\mathbf{x}^* \in \arg \min_{\mathbf{x} \in \mathcal{X}} \{f(\mathbf{x})\}$. Then, for any $\mathbf{y} \in \mathcal{X}$, we have

$$f(\mathbf{x}^*) \leq f(\mathbf{y}) - \frac{\mu}{2} \|\mathbf{y} - \mathbf{x}^*\|^2.$$

To proceed with our analysis, we first need to quantify the impact of one-step estimated gradient descent in terms of the squared gradient estimation error. This is given in the following lemma.

Lemma 2. Assume that $f(\mathbf{x}) : \mathcal{X} \rightarrow \mathbb{R}$ is a μ -strongly convex and L -smooth function. Let $\mathbf{z} \in \arg \min_{\mathbf{x} \in \mathcal{X}} \{\langle \nabla \hat{f}(\mathbf{y}), \mathbf{x} - \mathbf{y} \rangle + \frac{\alpha}{2} \|\mathbf{x} - \mathbf{y}\|^2\}$, where $\nabla \hat{f}(\mathbf{y})$ is an estimated gradient of $\nabla f(\mathbf{y})$, and $\mathbf{x}^* \in \arg \min_{\mathbf{x} \in \mathcal{X}} \{f(\mathbf{x})\}$. For any $\alpha \geq L$, and $\gamma \in (0, 2\mu)$, we have

$$\|\mathbf{z} - \mathbf{x}^*\|^2 \leq \eta \|\mathbf{y} - \mathbf{x}^*\|^2 + \beta \|\nabla \hat{f}(\mathbf{y}) - \nabla f(\mathbf{y})\|^2 \quad (14)$$

where $\eta = \frac{\alpha - \mu}{\alpha + \mu - \gamma} < 1$ and $\beta = \frac{1}{\gamma(\alpha + \mu - \gamma)}$.

Proof: See Appendix A.

Remark 6. From (14), the sufficient condition for $\|\mathbf{z} - \mathbf{x}^*\|^2 \leq \|\mathbf{y} - \mathbf{x}^*\|^2$ is $\|\nabla \hat{f}(\mathbf{y}) - \nabla f(\mathbf{y})\|^2 < \gamma(2\mu - \gamma) \|\mathbf{y} - \mathbf{x}^*\|^2$. This condition on the gradient estimation error is most easily satisfied when $\gamma = \mu$. In this case, the contraction constant $\eta = \frac{\alpha - \mu}{\alpha}$ recovers the one in [8]. Furthermore, as γ approaches 0, η approaches the contraction constant $\frac{\alpha - \mu}{\alpha + \mu}$ in [9]. Different from Proposition 2 in [8] and Lemma 5 in [9], Lemma 2 takes into account the impacts of estimated gradient descent and recovers the results in [8] and [9] as special cases.

Remark 7. To show a contraction relationship, the optimal gradient descent step-size in [10] needs to be in a specific range based on the knowledge of μ in (10), L in (11), and ν from an additional assumption $\|\nabla \hat{f}_t(\mathbf{x}_t) - \nabla f_t(\mathbf{x}_t)\|^2 \leq \epsilon^2 + \nu^2 \|\nabla f_t(\mathbf{x}_t)\|^2$ for some $\epsilon \geq 0$ and $\nu \geq 0$. The contraction analysis in [11] focuses on the proximal point algorithm and is substantially different from Lemma 2.

Leveraging Lemmas 1 and 2, we examine the impact of hierarchical multi-step gradient descent with estimated gradients on the dynamic regret bounds for OCO. The following theorem provides two upper bounds on the dynamic regret RE_T^d for HiOCO.

Theorem 3. For any $\alpha \geq L$, $\xi > 0$ and $\gamma \in (0, 2\mu)$, the dynamic regret yielded by HiOCO is bounded as follows:

i) For any $J_1 + J_r \geq 1$, we have

$$\text{RE}_T^d \leq \tau_r D R + \frac{D}{1 - \sqrt{\eta^{J_1 + J_r}}} \left(\tau_r R + \tau_r \Pi_T^* + \frac{\sqrt{\beta}}{1 - \sqrt{\eta}} \Delta_T \right).$$

ii) For any $J_1 + J_r \geq 1$ such that $2\eta^{J_1 + J_r} < 1$, we have

$$\begin{aligned} \text{RE}_T^d &\leq \frac{1}{2\xi} \sum_{t=1}^T \|\nabla f_t(\mathbf{x}_t^*)\|^2 + \frac{L + \xi}{2} \tau_r R^2 \\ &\quad + \frac{L + \xi}{2(1 - 2\eta^{J_1 + J_r})} \left(\tau_r R^2 + 2\tau_r^2 \Pi_{2,T}^* + \frac{2\beta}{1 - \eta} \Delta_{2,T} \right). \end{aligned}$$

Proof: See Appendix B.

Remark 8. The dynamic regret bounds in Theorem 3 hold for any general gradient estimation schemes that can be used in HiOCO. Note that in the definitions of Δ_T in (6) and $\Delta_{2,T}$ in (7), $\max_{\mathbf{x} \in \mathcal{X}} \{\|\nabla f_t(\mathbf{x}) - \nabla \hat{f}_t(\mathbf{x})\|\}$ is the maximum gradient estimation error w.r.t. some general gradient estimation function $\nabla \hat{f}(\cdot)$. Therefore, it serves as an upper bound for the gradient estimations in (8) and (9).

C. Discussion on the Dynamic Regret Bounds

In this section, we discuss the sufficient conditions for HiOCO to yield sublinear dynamic regret and highlight several prominent advantages of HiOCO over existing OCO algorithms.

We note that $\sum_{t=1}^T \|\nabla f_t(\mathbf{x}_t^*)\|^2$ is often small. In particular, if \mathbf{x}_t^* is an interior point of \mathcal{X} or **P1** is an unconstrained online problem, we readily have $\nabla f_t(\mathbf{x}_t^*) = \mathbf{0}$. For example, later in Section VI-B, we show that $\sum_{t=1}^T \|\nabla f_t(\mathbf{x}_t^*)\|^2 = 0$ for our application of online multi-TRP cooperative precoding design. Therefore, we usually have $\sum_{t=1}^T \|\nabla f_t(\mathbf{x}_t^*)\|^2 = \mathcal{O}(\min\{\Pi_T^*, \Pi_{2,T}^*\})$ [9]. In this case, we can simplify Theorem 3 to the following:

Corollary 4. Suppose $\sum_{t=1}^T \|\nabla f_t(\mathbf{x}_t^*)\|^2 = \mathcal{O}(\min\{\Pi_T^*, \Pi_{2,T}^*\})$. For any $J_1 + J_r \geq 1$ such that $2\eta^{J_1 + J_r} < 1$, we have

$$\text{RE}_T^d = \mathcal{O} \left(\min \left\{ \max\{\tau_r \Pi_T^*, \Delta_T\}, \max\{\tau_r^2 \Pi_{2,T}^*, \Delta_{2,T}\} \right\} \right).$$

Note that the feedback delay is always bounded by some constant in practice, i.e., $\tau_r = \mathcal{O}(1)$. Thus, from Corollary 4, a sufficient condition for HiOCO to yield sublinear dynamic regret is either $\max\{\Pi_T^*, \Delta_T\} = \mathbf{o}(T)$ or $\max\{\Pi_{2,T}^*, \Delta_{2,T}\} = \mathbf{o}(T)$, i.e., the variation measures grow sublinearly over time.

Remark 9. Sublinearity of the variation measures is necessary to have sublinear dynamic regret [28]. This can be seen from the dynamic regret bounds derived in [2], [7]-[11], [21]-[23] as shown in Table I. In many online applications, the system tends to stabilize over time, leading to sublinear system variation and thus sublinear dynamic regret.

We show in the following that the dynamic regret of HiOCO recovers or improves over the ones in [8]-[11].⁸

Remark 10. The centralized single-step and multi-step gradient descent algorithms achieve $\mathcal{O}(\Pi_T^*)$ and $\mathcal{O}(\min\{\Pi_T^*, \Pi_{2,T}^*\})$ dynamic regret in [8] and [9], respectively. If we configure HiOCO to perform gradient descent only at the master node, and assume one-slot delayed

⁸Existing works on distributed OCO [14]-[23] are limited to separable cost functions and thus cannot solve our online problem. Therefore, the dynamic regret bounds derived in [14]-[23] are not comparable with ours.

accurate data as in [8] and [9], the resulting dynamic regrets recover the ones in [8] and [9] as special cases.

Remark 11. The centralized single-step inexact gradient descent algorithms in [10] and [11] achieves $\mathcal{O}(\max\{\Pi_T^*, \Delta_T\})$ dynamic regret with one-slot delay. By configuring HiOCO to perform single-step gradient descent only at the master node, and assuming one-slot delayed inexact data as in [10] and [11], HiOCO recovers the dynamic regret bound in [10] and [11] as a special case. If the master node performs multi-step gradient descent, HiOCO yields an improved $\mathcal{O}(\min\{\max\{\Pi_T^*, \Delta_T\}, \max\{\Pi_{2,T}^*, \Delta_{2,T}\}\})$ dynamic regret compared with [10] and [11].

V. EXTENSION TO NON-ZERO LOCAL DELAY

We now consider the case of non-zero local delay, *i.e.*, at the beginning of each time slot t , each worker node c only has the τ_1 -delayed local data $\mathbf{d}_{t-\tau_1}^c$ for some $\tau_1 > 0$. Let $\tau = \tau_1 + \tau_r$ be the total delay. We extend Algorithms 1 and 2 to deal with non-zero local delay as follows.

In Algorithm 1, we make the following modifications: i) start the algorithm at $t > \tau$ in Step 2; ii) change $\mathbf{d}_{t-\tau}^c$ to $\mathbf{d}_{t-\tau}^c$ in Steps 2 and 3; iii) modify $\hat{\mathbf{d}}_{t-\tau}^c$ to $\hat{\mathbf{d}}_{t-\tau}^c$ in Steps 4 and 10; iv) set $\hat{\mathbf{x}}_t^{c,0} = \mathbf{x}_{t-\tau}^c$ in Step 5;⁹ v) construct gradient $\nabla \hat{f}_{t-\tau}^c(\hat{\mathbf{x}}_t^{c,j-1})$ in (8) with $\hat{\mathbf{d}}_{t-\tau}^c$ and $\hat{\mathbf{d}}_{t-\tau}^l$ replaced by $\hat{\mathbf{d}}_{t-\tau}^c$ and $\hat{\mathbf{d}}_{t-\tau}^l$, respectively, in Step 7; and vi) solve **P2** with gradient $\nabla \hat{f}_{t-\tau}^c(\hat{\mathbf{x}}_t^{c,j-1})$ instead of $\nabla \hat{f}_{t-\tau}^c(\hat{\mathbf{x}}_t^{c,j-1})$ in Step 8.

We make the following changes to Algorithm 2: i) start the algorithm at $t > \tau$ in Step 2; ii) change $\hat{\mathbf{d}}_{t-\tau}^l$ to $\hat{\mathbf{d}}_{t-\tau}^l$ in Step 3; iii) construct gradient $\nabla \hat{f}_{t-\tau}^c(\hat{\mathbf{x}}_t^{c,j-1})$ in (9) with \mathbf{d}_t^c and $\hat{\mathbf{d}}_{t-\tau}^l$ replaced by $\mathbf{d}_{t-\tau_1}^c$ and $\hat{\mathbf{d}}_{t-\tau}^l$, respectively, in Step 6; v) solve **P3** with gradient $\nabla \hat{f}_{t-\tau_1}^c(\hat{\mathbf{x}}_t^{c,j-1})$ instead of $\nabla \hat{f}_t^c(\hat{\mathbf{x}}_t^{c,j-1})$ in Step 7; and iv) modify \mathbf{d}_t^c to $\mathbf{d}_{t-\tau_1}^c$ in Step 10.

Using similar techniques as those in the proof of Theorem 3, we provide dynamic regret bounds for HiOCO in the presence of both local and remote delay.

Theorem 5. For any $\alpha \geq L$, $\xi > 0$ and $\gamma \in (0, 2\mu)$, the dynamic regret yielded by HiOCO is bounded as follows:

- i) For any $J_1 + J_r \geq 1$, the bound in claim i) of Theorem 3 still holds by replacing τ_r with τ .
- ii) For any $J_1 + J_r \geq 1$ such that $4\eta^{J_1+J_r} < 1$, we have

$$\begin{aligned} \text{RE}_T^d &\leq \frac{1}{2\xi} \sum_{t=1}^T \|\nabla f_t(\mathbf{x}_t^*)\|^2 + \frac{L+\xi}{2} \tau R^2 \\ &\quad + \frac{L+\xi}{2(1-4\eta^{J_1+J_r})} \left(\tau R^2 + 6\tau^2 \Pi_{2,T}^* + \frac{4\beta}{1-\eta} \Delta_{2,T} \right). \end{aligned}$$

Proof: See Appendix C.

Due to the additional local delay, Theorem 5 has a more stringent condition on the total number of gradient descent steps in claim ii) compared with the one in Theorem 3. However, the order of the dynamic regret bound is still dominated by the accumulated system variation measures and

⁹A more recent decision vector $\mathbf{x}_{t-\tau_1}^c$ than the dataset $\hat{\mathbf{d}}_{t-\tau}^c$ at the master node does not help to make a more accurate gradient estimation. Therefore, the timeliness of the local decision vector $\mathbf{x}_{t-\tau_1}^c$ is not useful at the master node.

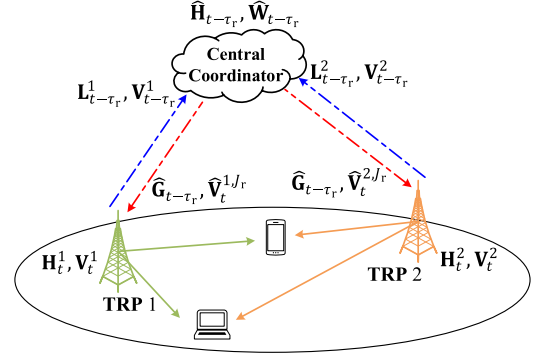


Fig. 2. An illustration of multi-TRP cooperative network with non-ideal backhaul communication links (showing the case of zero local delay for illustration).

is the same as the case without local delay. In particular, Theorem 5 implies that Corollary 4 still holds for the case of non-zero local delay by replacing τ_r with τ .

VI. APPLICATION TO MULTI-TRP COOPERATIVE WIRELESS NETWORKS

In practical wireless systems, the CSI is only available after channel acquisition and feedback. This challenge is especially acute with multiple-input multiple-output (MIMO) fading channels, where the channel can have a large state space and may fluctuate quickly over time. Online learning provides the tools to solve various online problems in dynamic MIMO systems.

We apply HiOCO to solve an online multi-TRP cooperative precoding design problem in MIMO systems, where multiple TRPs jointly transmit signals to serve all users in the network. Traditional cooperative precoding schemes focused on centralized offline problems with instantaneous CSI [29]-[31]. The TRPs defined in 5G NR are much smaller in size compared with the traditional base stations (BSs) and therefore have limited computation power. Furthermore, their backhaul communication links often have limited capacity in practice.

In prior works, online learning has been applied to dynamic MIMO systems in various forms, *e.g.*, [32]-[34]. Closer to our work, [35] and [36] studied online precoding designs for wireless network virtualization. However, they focused on centralized precoding problems in a single-cell scenario. In contrast, our precoding solution is updated at both the TRPs and the central coordinator in a hierarchical cooperative network.

A. Online Multi-TRP Cooperative Precoding Design

We consider a total of C TRPs coordinated by a central coordinator to jointly serve K users in the cooperative network as shown in Fig. 2. This is a special case of the general model shown in Fig. 1, where the TRPs correspond to the workers, and the central coordinator corresponds to the master.

Each TRP c has N^c antennas, for a total of $N = \sum_{c=1}^C N^c$ antennas in the network. Let $\mathbf{H}_t^c \in \mathbb{C}^{K \times N^c}$ denote the local channel state between the K users and TRP c . Let $\mathbf{H}_t = [\mathbf{H}_t^1, \dots, \mathbf{H}_t^C] \in \mathbb{C}^{K \times N}$ denote the global channel state between the K users and all TRPs. For ease of illustration, we

will describe this system assuming there is no local delay for the TRPs to collect the local CSI. The extension to non-zero local delay has been explained in Section V, and numerical results on that case will be provided in Section VII.

At each time slot t , each TRP c observes the current local CSI \mathbf{H}_t^c . The TRP's main function is to determine its own local precoding matrix $\mathbf{V}_t^c \in \mathbb{C}^{N^c \times K}$ to execute MIMO signal transmission to the K users. Note that \mathbf{V}_t^c must be in the convex set

$$\mathcal{V}^c \triangleq \{\mathbf{V}^c : \|\mathbf{V}^c\|_F^2 \leq P_{\max}^c\}, \quad (15)$$

which sets the maximum transmit power limit. Let $\mathbf{V}_t = [\mathbf{V}_t^1, \dots, \mathbf{V}_t^C]^H \in \mathbb{C}^{N \times K}$ denote the global precoding matrix executed by all TRPs at time slot t . The *actual* received signal vector \mathbf{y}_t (excluding noise) at the K users is given by

$$\mathbf{y}_t = \mathbf{H}_t \mathbf{V}_t \mathbf{s}_t$$

where $\mathbf{s}_t \in \mathbb{C}^{K \times 1}$ contains the transmitted signals from the TRPs to all K users, which are assumed to be independent to each other with unit power, *i.e.*, $\mathbb{E}\{\mathbf{s}_t \mathbf{s}_t^H\} = \mathbf{I}, \forall t$.

Ideally, the TRPs should collaborate in designing \mathbf{V}_t to achieve some joint communication objective, *e.g.*, cooperative zero-forcing (ZF) precoding from all TRP antennas to all users to remove inter-user interference [37]. However, that would require each TRP to have the CSI of all TRPs, which would be prohibitively expensive to accomplish. Therefore, a common solution is to use a central coordinator to collect the CSI and help designing \mathbf{V}_t .

1) *Backhaul Link without Delay*: To describe the interaction between the central coordinator and the TRPs, let us first consider idealized backhaul communication links, where each TRP c communicates \mathbf{H}_t^c to the central coordinator without delay. The central coordinator then has the global CSI \mathbf{H}_t at time slot t and designs a desired global precoder $\mathbf{W}_t \in \mathbb{C}^{N \times K}$ in $\cup_{c=1}^C \{\mathcal{V}^c\}$ to meet the per-TRP maximum power limits. Note that the design of \mathbf{W}_t can be based on the service needs of the K users and is not limited to any specific precoding scheme. The *desired* received signal vector (noiseless) $\tilde{\mathbf{y}}_t$ is given by

$$\tilde{\mathbf{y}}_t = \mathbf{H}_t \mathbf{W}_t \mathbf{s}_t.$$

With the TRPs' actual precoding matrix \mathbf{V}_t and the desired precoder \mathbf{W}_t at the central coordinator, the expected deviation of the actual received signal vector at all K users from the desired one is given by $\mathbb{E}\{\|\mathbf{y}_t - \tilde{\mathbf{y}}_t\|_F^2\} = \|\mathbf{H}_t \mathbf{V}_t - \mathbf{H}_t \mathbf{W}_t\|_F^2$. Therefore, we define the precoding deviation of the TRPs' precoding from the precoder at the central coordinator as

$$f_t(\mathbf{V}) \triangleq \|\mathbf{H}_t \mathbf{V} - \mathbf{H}_t \mathbf{W}_t\|_F^2, \quad \forall t. \quad (16)$$

We note that $f_t(\mathbf{V})$ naturally quantifies the difference between the idealized global precoder determined by the central coordinator and the actual local precoders executed at the distributed TRPs. Furthermore, it is strongly convex in \mathbf{V} .

The goal of the multi-TRP cooperative network is to minimize the accumulation of precoding deviation $f_t(\mathbf{V}_t)$ subject to per-TRP maximum transmit power limits with non-ideal backhaul communication links. This online optimization

problem is in the same form as **P1** with $\{\mathbf{H}_t^c\}_{c=1}^C$ being the local data, $\{\mathbf{V}_t^c \in \mathcal{V}^c\}_{c=1}^C$ being the local decisions, and $f_t(\mathbf{V})$ being the global cost function.

Remark 12. Note that due to the coupling of local channel states $\{\mathbf{H}_t^c\}_{c=1}^C$ and local precoders $\{\mathbf{V}_t^c\}_{c=1}^C$, the cost function $f_t(\mathbf{V})$ is not separable among the TRPs. Furthermore, the local gradient at each TRP c depends on the local channel state \mathbf{H}_t^c , local precoder \mathbf{V}^c , and the channel states $\{\mathbf{H}_t^l\}_{l \neq c}$ and precoders $\{\mathbf{V}^l\}_{l \neq c}$ at the other TRPs. It is given by

$$\nabla f_t^c(\mathbf{V}) \triangleq \frac{\partial f_t(\mathbf{V})}{\partial \mathbf{V}^{c*}} = \mathbf{H}_t^{cH} \left(\sum_{l=1}^C (\mathbf{H}_t^l \mathbf{V}^l) - \mathbf{H}_t \mathbf{W}_t \right). \quad (17)$$

2) *Backhaul Link with Delay*: For the general case of non-ideal backhaul links, at each time slot t , there is a delay in sending the timely local CSI \mathbf{H}_t^c from each TRP c to the central coordinator. As illustrated in Section IV-A, for non-ideal backhaul links with τ_r^u -slot uplink delay and τ_r^d -slot downlink delay, only the round-trip delay τ_r matters. Therefore, without loss of generality, we simply assume there is τ_r -slot uplink delay but no downlink delay. If communication overhead is a concern, instead of sending the exact local CSI \mathbf{H}_t^c , each TRP c can send a compressed version of the local CSI, denoted by \mathbf{L}_t^c , to the central coordinator. In this case, the central coordinator recovers a delayed global channel state $\hat{\mathbf{H}}_{t-\tau_r}$ with some errors, and then it designs the desired global precoding matrix $\hat{\mathbf{W}}_{t-\tau_r}$. In Section VI-B, we will show how HiOCO leverages the instantaneous local CSI $\{\mathbf{H}_t^c\}_{c=1}^C$ at the TRPs and the delayed global CSI $\hat{\mathbf{H}}_{t-\tau_r}$ at the central coordinator to jointly design the cooperative precoding matrices $\{\mathbf{V}_t^c\}_{c=1}^C$.

Remark 13. The optimal global precoding solution is $\mathbf{V}_t^* = \mathbf{W}_t$ at each time slot t . However, with non-ideal backhaul links, the TRPs cannot receive \mathbf{V}_t^* from the central coordinator in time and execute it at each time slot t . A naive solution is to execute the delayed optimal solution $\mathbf{V}_{t-\tau_r}^*$ at the TRPs. However, In Section VII, we will show that directly executing $\mathbf{V}_{t-\tau_r}^*$ at the TRPs leads to system performance degradation compared with HiOCO, which can utilize the more timely CSI at the TRPs.

B. Hierarchical Precoding Solution

We now describe how to use HiOCO to generate a solution to the above online multi-TRP cooperative precoding design problem.

1) *Precoding Solution at Central Coordinator*: At the beginning of each time slot t , the central coordinator receives the precoding matrices $\{\mathbf{V}_{t-\tau_r}^c\}_{c=1}^C$ from the TRPs and recovers the delayed global CSI $\hat{\mathbf{H}}_{t-\tau_r}$ with some errors from the compressed local CSI $\{\mathbf{L}_{t-\tau_r}^c\}_{c=1}^C$. It then sets $\hat{\mathbf{V}}_t^{c,0} = \mathbf{V}_{t-\tau_r}^c$ for each TRP c and performs J_r -step estimated gradient descent to generate $\hat{\mathbf{V}}_t^{c,J_r}$. For each gradient descent step $j \in \{1, \dots, J_r\}$, the central coordinator has a closed-form precoding solution, given by

$$\hat{\mathbf{V}}_t^{c,j} = \mathcal{P}_{\mathcal{V}^c} \left\{ \hat{\mathbf{V}}_t^{c,j-1} - \frac{1}{\alpha} \nabla f_{t-\tau_r}^c(\hat{\mathbf{V}}_t^{c,j-1}) \right\} \quad (18)$$

where $\mathcal{P}_{\mathcal{V}^c}\{\mathbf{V}^c\} \triangleq \arg \min_{\mathbf{U}^c \in \mathcal{V}^c} \{\|\mathbf{U}^c - \mathbf{V}^c\|_F^2\}$ is the projection operator onto the convex feasible set \mathcal{V}^c and

$$\nabla \hat{f}_{t-\tau_r}^c(\hat{\mathbf{V}}_t^{c,j-1}) = \hat{\mathbf{H}}_{t-\tau_r}^{cH} \left(\sum_{l=1}^C \left(\hat{\mathbf{H}}_{t-\tau_r}^l \hat{\mathbf{V}}_t^{l,j-1} \right) - \hat{\mathbf{H}}_{t-\tau_r} \hat{\mathbf{W}}_{t-\tau_r} \right)$$

is an estimation of the delayed gradient. The central coordinator then communicates the intermediate precoder $\hat{\mathbf{V}}_t^{c,J_r}$ and global information

$$\hat{\mathbf{G}}_{t-\tau_r}^c = \sum_{l=1, l \neq c}^C \left(\hat{\mathbf{H}}_{t-\tau_r}^l \hat{\mathbf{V}}_t^{l,J_r} \right) - \hat{\mathbf{H}}_{t-\tau_r} \hat{\mathbf{W}}_{t-\tau_r} \in \mathbb{C}^{K \times K}$$

to each TRP c .

2) *Precoding Solution at TRP c* : At the beginning of each time slot t , after receiving the intermediate precoder $\hat{\mathbf{V}}_t^{c,J_r}$ and global information $\hat{\mathbf{G}}_{t-\tau_r}^c$ from the central coordinator, each TRP c sets $\tilde{\mathbf{V}}_t^{c,0} = \hat{\mathbf{V}}_t^{c,J_r}$ and performs J_1 -step estimated gradient descent to generate $\tilde{\mathbf{V}}_t^{c,J_1}$. For each gradient descent step $j \in \{1, \dots, J_1\}$, each TRP c also has a closed-form precoding solution, given by

$$\tilde{\mathbf{V}}_t^{c,j} = \mathcal{P}_{\mathcal{V}^c} \left\{ \tilde{\mathbf{V}}_t^{c,j-1} - \frac{1}{\alpha} \nabla \hat{f}_t^c(\tilde{\mathbf{V}}_t^{c,j-1}) \right\} \quad (19)$$

where

$$\nabla \hat{f}_t^c(\tilde{\mathbf{V}}_t^{c,j-1}) = \mathbf{H}_t^{cH} \left(\mathbf{H}_t^c \tilde{\mathbf{V}}_t^{c,j-1} + \hat{\mathbf{G}}_{t-\tau_r}^c \right)$$

is an estimation of the current gradient based on the most recent local CSI \mathbf{H}_t^c and the delayed global information $\hat{\mathbf{G}}_{t-\tau_r}^c$. Finally, each TRP c uses $\mathbf{V}_t^c = \tilde{\mathbf{V}}_t^{c,J_1}$ as its precoding matrix for transmission at each time slot t and communicates it together with either the complete local CSI \mathbf{H}_t^c or the compressed local CSI \mathbf{L}_t^c to the central coordinator.

Remark 14. Per-antenna power constraints at each TRP c can be incorporated into the convex set \mathcal{V}^c . In this case, we still have closed-form solutions similar to (18) and (19) with the projection operator redefined w.r.t. per-antenna power limits.

3) *Communication and Computation Complexity*: If the master node sends $\hat{\mathbf{H}}_{t-\tau_r}$, $\hat{\mathbf{V}}_t^{J_r}$, and $\hat{\mathbf{W}}_{t-\tau_r}$ to TRP c for local gradient estimation, the amount of communication overhead is $3NK$. By communicating $\hat{\mathbf{V}}_t^{c,J_r}$ and $\hat{\mathbf{G}}_{t-\tau_r}^c$ to TRP c , the amount overhead reduces to $(N^c + K)K$. Furthermore, there is no need to communicate $\hat{\mathbf{H}}_{t-\tau_r}^c$, $\hat{\mathbf{V}}_t^{c,J_r}$ to TRP c , since more recent local information will be used by the TRP to reduce the gradient estimation error.

The computational complexities of our hierarchical precoding solutions in (18) and (19) for each TRP c are dominated by matrix multiplications. They are in the order of $\mathcal{O}(NK^2)$ and $\mathcal{O}(N^c K^2)$, respectively.

4) *Performance Bounds*: We first observe that the channel power is always bounded in practice, *i.e.*, there exists some $B > 0$, such that $\|\mathbf{H}_t\|_F^2 \leq B$, for all t . In the following lemma, we show that the online multi-TRP cooperative precoding design problem satisfies Assumptions 1 and 2 made in Section IV-B. The proof follows from the above bound on \mathbf{H}_t , as well as the transmit power limits on \mathbf{V}_t and \mathbf{W}_t , and is omitted for brevity.

Lemma 6. Assumptions 1 and 2 hold with $\mu = 2$, $L = B$, $D = 2B \sqrt{\sum_{c=1}^C P_{\max}^c}$, and $R = 2 \sqrt{\sum_{c=1}^C P_{\max}^c}$.

Using the results in Theorems 3 and 5, and noting that the gradient at the optimal precoder satisfies $\nabla f_t(\mathbf{V}_t^*) = \mathbf{H}_t^H (\mathbf{H}_t \mathbf{V}_t^* - \mathbf{H}_t \mathbf{W}_t) = \mathbf{0}$, the following corollary provides the dynamic regret bounds yielded by our proposed hierarchical online precoding solution $\{\mathbf{V}_t\}_{t=1}^T$.

Corollary 7. The dynamic regret bounds in Theorems 3 and 5 hold for $\{\mathbf{V}_t\}_{t=1}^T$ generated by HiOCO, with the constants μ , L , D , and R given in Lemma 6 and $\sum_{t=1}^T \|\nabla f_t(\mathbf{V}_t^*)\|_F^2 = 0$.

VII. SIMULATION RESULTS

In this section, we present simulation results under typical urban micro-cell LTE network settings. We study the impacts of various system parameters on the convergence and performance of HiOCO. We numerically demonstrate the performance advantage of HiOCO over existing alternatives.

A. Simulation Setup

We consider an urban hexagon micro-cell of radius 500 m, with $C = 3$ equally separated TRPs. Each TRP c is equipped with $N^c = 16$ antennas as default. We consider 5 co-located users at the mid-point between every two adjacent TRPs, for a total of $K = 15$ users in the network by default. The impacts of N and K on the performance of HiOCO will be studied later.

Following the standard LTE specifications [38], we focus on the channel over one subcarrier of bandwidth $B_W = 15$ kHz. We set the maximum transmit power limit $P_{\max}^c = 30$ dBm for all c , noise power spectral density $N_0 = -174$ dBm/Hz, and noise figure $N_F = 10$ dB. We model the fading channel as a first-order Gauss-Markov process [39] $\mathbf{h}_{t+1}^{c,k} = \alpha_h \mathbf{h}_t^{c,k} + \mathbf{z}_t^{c,k}$ between TRP c and user k , where $\alpha_h \in [0, 1]$ is the channel correlation coefficient, $\mathbf{h}_t^{c,k} \sim \mathcal{CN}(\mathbf{0}, \beta^{c,k} \mathbf{I})$ with $\beta^{c,k}$ representing the large-scale fading variation consisting of the path-loss and shadowing, and $\mathbf{z}_t^{c,k} \sim \mathcal{CN}(\mathbf{0}, (1 - \alpha_h^2) \beta^{c,k} \mathbf{I})$ is independent of $\mathbf{h}_t^{c,k}$. We model $\beta^{c,k}$ as [38] $\beta^{c,k}[\text{dB}] = -31.54 - 33 \log_{10}(d^{c,k}) - \psi^{c,k}$, where $d^{c,k}$ is the distance in kilometers from TRP c to user k , and $\psi^{c,k} \sim \mathcal{CN}(0, \sigma_\phi^2)$ is the shadowing effect that is used to model the variation of user positions with $\sigma_\phi^2 = 8$ dB. We set $\alpha_h = 0.998$ as default, which corresponds to user speed 1 km/h.

We assume each TRP c communicates the exact local CSI \mathbf{H}_t^c to the central coordinator, since the impact of channel compression error can be emulated by increasing the communication delay τ_r under the Gauss-Markov channel model. Furthermore, we emphasize here that the Gauss-Markov channel model is used for illustration only. HiOCO can be applied to any arbitrary wireless environment, and neither the TRPs nor the central coordinator needs to know the channel statistics.

We assume the central coordinator adopts cooperative ZF precoding as its desired precoder, given by

$$\mathbf{W}_t^{\text{ZF}} = \sqrt{P_t^{\text{ZF}}} \mathbf{H}_t^H (\mathbf{H}_t \mathbf{H}_t^H)^{-1}$$

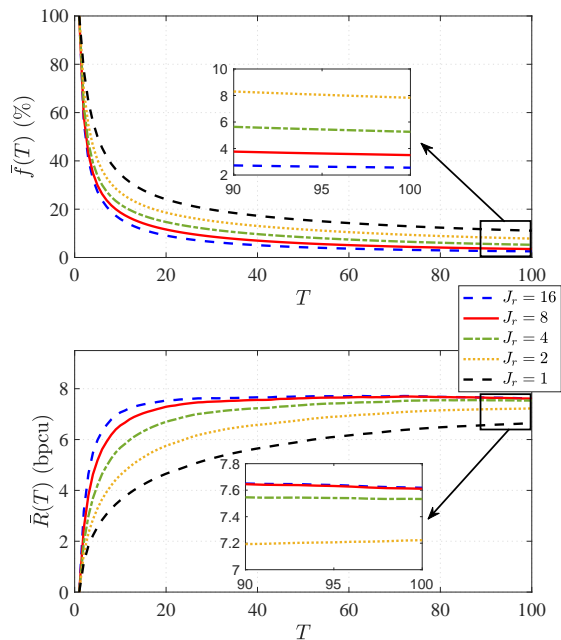


Fig. 3. $\bar{f}(T)$ and $\bar{R}(T)$ vs. T with $J_1 = 1$ and different J_r values.

where P_t^{ZF} is a power normalizing factor. Note that we must have $N \geq K$ to perform ZF precoding. We assume all K users have the same noise power $\sigma_n^2 = N_F + N_0 B_W$ and therefore all the users will have the same data rate $\log_2(1 + \frac{P_t^{\text{ZF}}}{\sigma_n^2})$ by using \mathbf{W}_t^{ZF} . The central coordinator adopts the following power normalizing factor

$$P_t^{\text{ZF}*} = \min \left\{ \frac{P_{\max}^c}{\|\mathbf{H}_t^{cH}(\mathbf{H}_t \mathbf{H}_t^H)^{-1}\|_F^2}, \forall c \right\},$$

which is the optimal solution for the following sum rate maximization problem with per-TRP maximum transmit power limits, given by:

$$\begin{aligned} \mathbf{P4} : \quad & \max_{P_t^{\text{ZF}} \geq 0} K \log_2 \left(1 + \frac{P_t^{\text{ZF}}}{\sigma_n^2} \right) \\ & \text{s.t.} \quad P_t^{\text{ZF}} \|\mathbf{H}_t^{cH}(\mathbf{H}_t \mathbf{H}_t^H)^{-1}\|_F^2 \leq P_{\max}^c, \quad \forall c. \end{aligned}$$

As performance metrics, we define the time-averaged normalized precoding deviation as

$$\bar{f}(T) \triangleq \frac{1}{T} \sum_{t=1}^T \frac{f_t(\mathbf{V}_t)}{\|\mathbf{H}_t \mathbf{W}_t^{\text{ZF}}\|_F^2}$$

and the time-averaged per-user rate as

$$\bar{R}(T) \triangleq \frac{1}{TK} \sum_{t=1}^T \sum_{k=1}^K \log_2(1 + \text{SINR}_t^k)$$

where $\text{SINR}_t^k = \frac{|\mathbf{H}_t \mathbf{V}_t|_{k,k}|^2}{\sum_{j \neq k} |\mathbf{H}_t \mathbf{V}_t|_{k,j}|^2 + \sigma_n^2}$ is the signal-to-interference-plus-noise-ratio of user k at time slot t .

B. Performance Comparison Benchmarks

For performance comparison, we consider the following benchmarks.

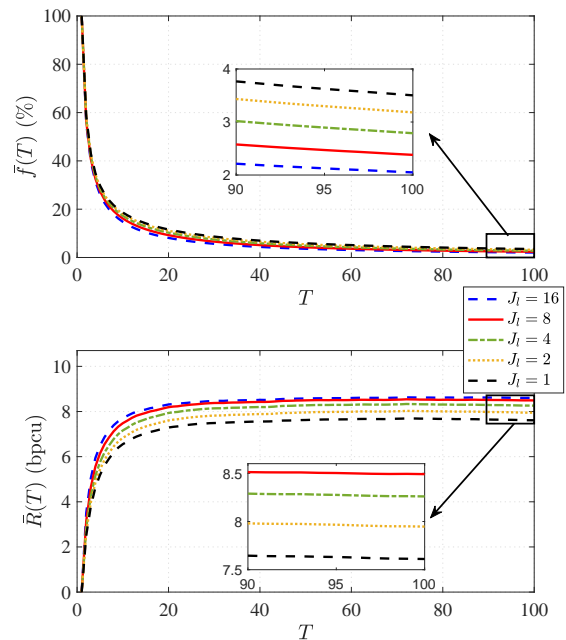
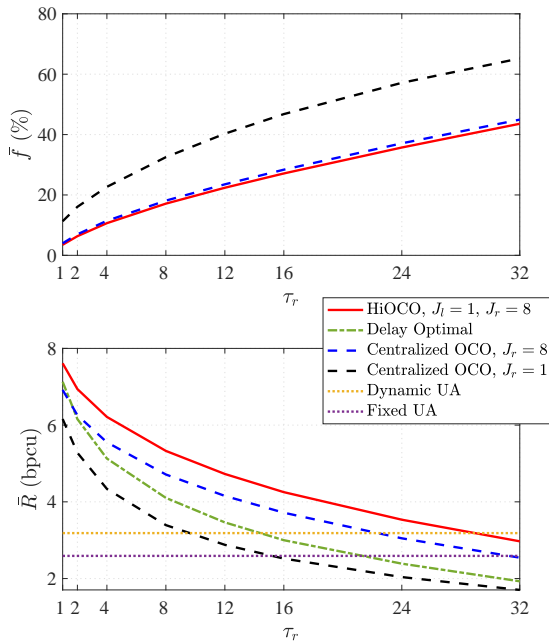
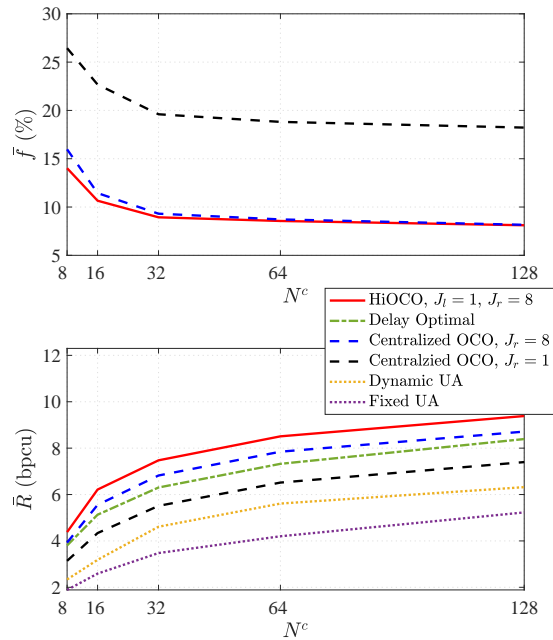
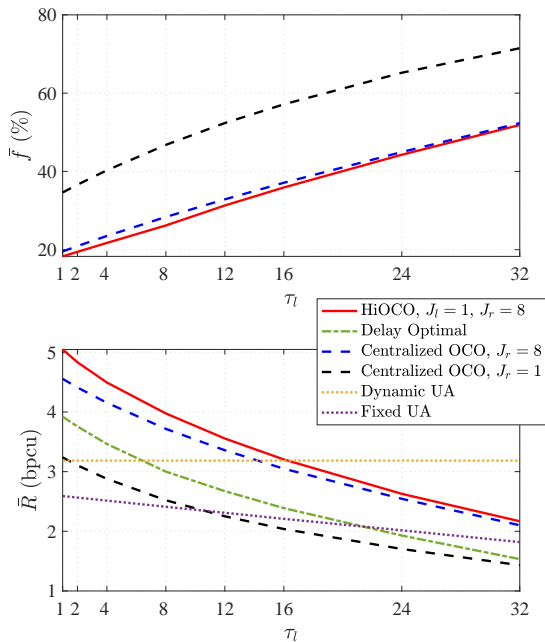
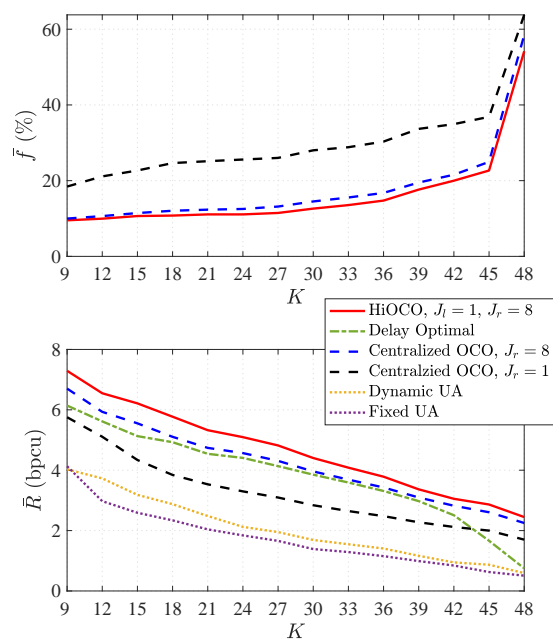


Fig. 4. $\bar{f}(T)$ and $\bar{R}(T)$ vs. T with $J_r = 8$ and different J_1 values.

- *Delay Optimal*: The central coordinator collects CSI from all TRPs, computes the optimal global precoder, and sends it to all TRPs. However, due to the local and remote delays, what the TRPs actually execute is the precoder $\mathbf{V}_{t-\tau_1-\tau_r}^* = \mathbf{W}_{t-\tau_1-\tau_r}^{\text{ZF}}$ that can be received from the central coordinator at each time slot $t > \tau_1 + \tau_r$.
- *Centralized OCO*: We run Algorithm 1 at the central coordinator with different numbers of gradient descent steps J_r , which can be viewed as instances of the centralized OCO algorithms in [8]-[11]. At each time slot $t > \tau_1 + \tau_r$, the TRPs execute the precoder $\hat{\mathbf{V}}_{t-\tau_1-\tau_r}^{J_r}$ received from the central coordinator, without performing any local gradient descent.
- *Dynamic User Association (UA)*: Since distributed OCO is not applicable to our problem, we consider the following distributed scheme. Each user k selects the TRP that has the highest channel gain for downlink signal transmission at each time slot t based on the τ_1 -slot delayed local CSI $\mathbf{H}_{t-\tau_1}^c$. Let the number of users associated with TRP c be $K_{t-\tau_1}^c$. Let $\tilde{\mathbf{H}}_{t-\tau_1}^c \in \mathbb{C}^{K_{t-\tau_1}^c \times N^c}$ denote the available channel state between the $K_{t-\tau_1}^c$ users and TRP c at each time slot $t > \tau_1$. Each TRP c adopts ZF precoding to serve the $K_{t-\tau_1}^c$ users at each time slot $t > \tau_1$, given by $\sqrt{\tilde{P}_{t-\tau_1}^c} \tilde{\mathbf{H}}_{t-\tau_1}^{cH} (\tilde{\mathbf{H}}_{t-\tau_1}^c \tilde{\mathbf{H}}_{t-\tau_1}^{cH})^{-1}$, where $\tilde{P}_{t-\tau_1}^c$ is set such that $\|\tilde{\mathbf{V}}_{t-\tau_1}^c\|_F^2 = P_{\max}^c$.
- *Fixed UA*: This is a more realistic alternative to *Dynamic UA*. Each user k selects the TRP that has the lowest path loss. The user association does not change during our simulation. The TRPs operate in the same way as under *Dynamic UA*.

C. Impact of Number of Estimated Gradient Descent Steps

Fig. 3 and Fig. 4 show $\bar{f}(T)$ and $\bar{R}(T)$ versus T for different numbers of the estimated gradient descent steps J_r

Fig. 5. \bar{f} and \bar{R} vs. τ_r with $\tau_l = 0$.Fig. 7. \bar{f} and \bar{R} vs. N^c with $K = 15$.Fig. 6. \bar{f} and \bar{R} vs. τ_l with $\tau_r = 8$.Fig. 8. \bar{f} and \bar{R} vs. K with $N^c = 16$.

at the central coordinator and J_1 at the TRPs. We consider zero local delay first and set the remote delay as $\tau_r = 1$. We observe that HiOCO converges fast (within $T = 100$ time slots). Furthermore, the system performance improves as J_r or J_l increases, showing the performance gain brought by performing multi-step gradient descent with our proposed gradient estimations at either the central coordinator or the TRPs. As shown in Fig. 3, the system performance almost stabilizes when $J_r = 8$. Further considering the TRPs usually have less computation capacity compared with the central coordinator, we set $J_l = 1$ and $J_r = 8$ as default parameters in the simulation results presented below.

D. Impact of Remote and Local Delays

Fig. 5 and Fig. 6 show the performance comparison between HiOCO and the benchmarks. We study the steady state value of $\bar{f}(T)$ and $\bar{R}(T)$ versus the remote delay τ_r and local delay τ_l . Note that $\bar{f}(T)$ is relevant only to the OCO methods.

As shown in Fig. 5, for a wide range of remote delay values, HiOCO outperforms both *Dynamic UA* and *Fixed UA*. This demonstrates that even with large remote delay, it helps to utilize a central coordinator. Furthermore, HiOCO outperforms the centralized alternatives *Delay Optimal* and *Centralized OCO*, which demonstrates the importance of performing local gradient descent at the TRPs using more timely CSI. As shown

in Fig. 6, the performance gain of HiOCO over *Centralized OCO* decreases as the local delay τ_1 increases. It indicates the importance of information timeliness on the performance gain brought by the local gradient descent. Overall, we observe that, by taking fully advantage of the timely local CSI and delayed global CSI to perform gradient descent at both the TRPs and central coordinator, HiOCO outperforms existing alternatives over a wide range of delay scenarios.

E. Impact of Number of Antennas and Users

We further study the impact of the numbers of antennas N^c and users K . Fig. 7 shows that the steady-state precoding deviation \bar{f} decreases as the number of antennas N^c increases, since the TRPs have more degrees of freedom to design their cooperative precoding. The steady-state per-user rate \bar{R} dramatically improves as N^c increases, indicating the performance advantage of massive MIMO. Fig. 8 shows that the precoding deviation keeps increasing as the number of users K increases, due to the increased inter-user interference. Note that to perform cooperative precoding at the central coordinator, the number of users should be $K \leq N = 48$. We observe that HiOCO substantially outperforms *Delay Optimal* when the number of users is close to the number of antennas in the presence of multi-slot delay. Furthermore, in a wide range of N^c and K values, HiOCO yields the best performance among all alternatives.

VIII. CONCLUSIONS

We have studied a new OCO framework over a master-worker network, where the local data at the worker nodes may be non-independent or non-identically distributed, the global cost functions may be non-separable, and there may be multi-slot delay in both local data acquisition and the communication between the worker nodes and the master node. We propose the HiOCO algorithm, which takes full advantage of the network heterogeneity in information timeliness and computation capacity. HiOCO allows both timely local gradient descent at the local worker nodes and delayed global gradient descent at the remote master node. Furthermore, HiOCO allows multi-step estimated gradient descent at both the worker nodes and the master node to fully utilize their computation capacities. Our analysis considers the impacts of the unique hierarchical architecture, multi-slot delay, and gradient estimation error, on the performance guarantees of HiOCO in terms of dynamic regret bounds. We apply HiOCO to an online multi-TRP cooperative precoding design problem for 5G NR. Simulation results demonstrate the superior delay tolerance and substantial performance advantage of HiOCO over existing alternatives under a wide range of scenarios.

APPENDIX A PROOF OF LEMMA 2

Proof: Note that $\langle \nabla \hat{f}(\mathbf{y}), \mathbf{x} - \mathbf{y} \rangle + \frac{\alpha}{2} \|\mathbf{x} - \mathbf{y}\|^2$ is α -strongly convex. Applying Lemma 1, we have

$$\langle \nabla f(\mathbf{y}), \mathbf{z} - \mathbf{y} \rangle + \frac{\alpha}{2} \|\mathbf{z} - \mathbf{y}\|^2 + \langle \nabla \hat{f}(\mathbf{y}) - \nabla f(\mathbf{y}), \mathbf{z} - \mathbf{y} \rangle$$

$$\leq \langle \nabla f(\mathbf{y}), \mathbf{x}^* - \mathbf{y} \rangle + \frac{\alpha}{2} \|\mathbf{x}^* - \mathbf{y}\|^2 - \frac{\alpha}{2} \|\mathbf{z} - \mathbf{x}^*\|^2 + \langle \nabla \hat{f}(\mathbf{y}) - \nabla f(\mathbf{y}), \mathbf{x}^* - \mathbf{y} \rangle. \quad (20)$$

From $f(\mathbf{x})$ being L -smooth, we have

$$f(\mathbf{z}) \leq f(\mathbf{y}) + \langle \nabla f(\mathbf{y}), \mathbf{z} - \mathbf{y} \rangle + \frac{L}{2} \|\mathbf{z} - \mathbf{y}\|^2. \quad (21)$$

From $f_t(\mathbf{x})$ being μ -strongly convex, we have

$$f(\mathbf{x}^*) \geq f(\mathbf{y}) + \langle \nabla f(\mathbf{y}), \mathbf{x}^* - \mathbf{y} \rangle + \frac{\mu}{2} \|\mathbf{x}^* - \mathbf{y}\|^2. \quad (22)$$

Adding $f(\mathbf{y})$ on both sides of (20), and then applying (21) and (22) to the LHS and RHS of (20), respectively, we have

$$\begin{aligned} f(\mathbf{z}) - \frac{L}{2} \|\mathbf{z} - \mathbf{y}\|^2 + \frac{\alpha}{2} \|\mathbf{z} - \mathbf{y}\|^2 \\ \leq f(\mathbf{x}^*) - \frac{\mu}{2} \|\mathbf{y} - \mathbf{x}^*\|^2 + \frac{\alpha}{2} \|\mathbf{y} - \mathbf{x}^*\|^2 - \frac{\alpha}{2} \|\mathbf{z} - \mathbf{x}^*\|^2 \\ + \langle \nabla f(\mathbf{y}) - \nabla \hat{f}(\mathbf{y}), \mathbf{z} - \mathbf{x}^* \rangle. \end{aligned} \quad (23)$$

Applying Lemma 1 again, we have

$$f(\mathbf{x}^*) \leq f(\mathbf{z}) - \frac{\mu}{2} \|\mathbf{z} - \mathbf{x}^*\|^2. \quad (24)$$

Substituting (24) into the RHS of (23), noting that $\langle \mathbf{a}, \mathbf{b} \rangle \leq \frac{1}{2\gamma} \|\mathbf{a}\|^2 + \frac{\gamma}{2} \|\mathbf{b}\|^2$ for any $\gamma > 0$, multiplying both sides by 2, and rearranging terms, we have

$$\begin{aligned} (\alpha + \mu - \gamma) \|\mathbf{z} - \mathbf{x}^*\|^2 + (\alpha - L) \|\mathbf{z} - \mathbf{y}\|^2 \\ \leq (\alpha - \mu) \|\mathbf{y} - \mathbf{x}^*\|^2 + \frac{1}{\gamma} \|\nabla f(\mathbf{y}) - \nabla \hat{f}(\mathbf{y})\|^2. \end{aligned} \quad (25)$$

Note that the strong convexity constant μ is smaller than the constant of smoothness L , i.e., $\mu \leq L$ [8]. From (25), we have (14) for any $\alpha \geq L$ and $\gamma < 2\mu \leq \alpha + \mu$. ■

APPENDIX B PROOF OF THEOREM 3

Proof: We first prove claim i). We have

$$\begin{aligned} \text{RE}_T^d &= \sum_{t=1}^T (f_t(\mathbf{x}_t) - f_t(\mathbf{x}_t^*)) \stackrel{(a)}{\leq} \sum_{t=1}^T \langle \nabla f_t(\mathbf{x}_t), \mathbf{x}_t - \mathbf{x}_t^* \rangle \\ &\stackrel{(b)}{\leq} \sum_{t=1}^T \|\nabla f_t(\mathbf{x}_t)\| \|\mathbf{x}_t - \mathbf{x}_t^*\| \stackrel{(c)}{\leq} \tau_1 DR + D \sum_{t=\tau_r+1}^T \|\mathbf{x}_t - \mathbf{x}_t^*\|. \end{aligned} \quad (26)$$

where (a) follows from the convexity of $f_t(\mathbf{x})$; (b) is because $\langle \mathbf{a}, \mathbf{b} \rangle \leq \|\mathbf{a}\| \|\mathbf{b}\|$; and (c) follows from $\nabla f_t(\mathbf{x})$ and \mathcal{X} being bounded in (12) and (13), respectively.

We now bound $\sum_{t=\tau_r+1}^T \|\mathbf{x}_t - \mathbf{x}_t^*\|$ in (26). We have

$$\begin{aligned} \sum_{t=\tau_r+1}^T \|\mathbf{x}_t - \mathbf{x}_t^*\| \\ \stackrel{(a)}{\leq} \sqrt{\eta^{J_1}} \sum_{t=\tau_r+1}^T \left(\|\hat{\mathbf{x}}_t^{J_1} - \mathbf{x}_t^*\| \right) + \frac{1 - \sqrt{\eta^{J_1}}}{1 - \sqrt{\eta}} \sqrt{\beta} \Delta_T \end{aligned} \quad (27)$$

where (a) follows from applying Lemma 2 to **P3** for J_1 times, $\|\mathbf{a}\|^2 + \|\mathbf{b}\|^2 \leq (\|\mathbf{a}\| + \|\mathbf{b}\|)^2$ such that $\|\hat{\mathbf{x}}_t^{J_1} - \mathbf{x}_t^*\| \leq \sqrt{\eta} \|\hat{\mathbf{x}}_t^{J_1-1} - \mathbf{x}_t^*\| + \sqrt{\beta} \|\nabla f_t(\hat{\mathbf{x}}_t^{J_1-1}) - \nabla f_t(\hat{\mathbf{x}}_t^{J_1-1})\|$ for any

$j \in \{1, \dots, J_1\}$, and the definition of Δ_T in (6). We continue to bound $\sum_{t=\tau_r+1}^T \|\hat{\mathbf{x}}_t^{J_r} - \mathbf{x}_t^*\|$ in (27) as follows:

$$\begin{aligned} & \sum_{t=\tau_r+1}^T \|\hat{\mathbf{x}}_t^{J_r} - \mathbf{x}_t^*\| \\ & \stackrel{(a)}{\leq} \sum_{t=\tau_r+1}^T \left(\|\hat{\mathbf{x}}_t^{J_r} - \mathbf{x}_{t-\tau_r}^*\| + \|\mathbf{x}_t^* - \mathbf{x}_{t-\tau_r}^*\| \right) \\ & \stackrel{(b)}{\leq} \sum_{t=\tau_r+1}^T \left(\|\hat{\mathbf{x}}_t^{J_r} - \mathbf{x}_{t-\tau_r}^*\| \right) + \tau_r \Pi_T^* \\ & \stackrel{(c)}{\leq} \sqrt{\eta^{J_r}} \sum_{t=\tau_r+1}^T \left(\|\mathbf{x}_{t-\tau_r} - \mathbf{x}_{t-\tau_r}^*\| \right) + \tau_r \Pi_T^* + \frac{1 - \sqrt{\eta^{J_r}}}{1 - \sqrt{\eta}} \sqrt{\beta} \Delta_T \end{aligned} \quad (28)$$

where (a) is because $\|\mathbf{a} + \mathbf{b}\| \leq \|\mathbf{a}\| + \|\mathbf{b}\|$, (b) follows from the definition of Π_T^* in (4), and (c) follows from applying Lemma 2 to $\mathbf{P2}$ for J_r times similar to (a) in (27).

Substituting (28) into (27), noting that $\sum_{t=\tau_r+1}^T \|\mathbf{x}_{t-\tau_r} - \mathbf{x}_{t-\tau_r}^*\| \leq \sum_{t=1}^T \|\mathbf{x}_t - \mathbf{x}_t^*\|$, and rearranging terms, we have

$$\begin{aligned} & \left(1 - \sqrt{\eta^{J_1+J_r}}\right) \sum_{t=\tau_r+1}^T \|\mathbf{x}_t - \mathbf{x}_t^*\| - \sqrt{\eta^{J_1+J_r}} \sum_{t=1}^{\tau_r} \|\mathbf{x}_t - \mathbf{x}_t^*\| \\ & \leq \sqrt{\eta^{J_1}} \tau_r \Pi_T^* + \frac{\sqrt{\eta^{J_1}}(1 - \sqrt{\eta^{J_r}}) + 1 - \sqrt{\eta^{J_1}}}{1 - \eta} \sqrt{\beta} \Delta_T. \end{aligned} \quad (29)$$

Substituting (29) into (26) and noting that $\eta < 1$ and the radius of \mathcal{X} being bounded in (13), we prove claim i).

We now prove claim ii). We have

$$\begin{aligned} \text{RE}_T^d &= \sum_{t=1}^T (f_t(\mathbf{x}_t) - f_t(\mathbf{x}_t^*)) \\ & \stackrel{(a)}{\leq} \sum_{t=1}^T \left(\langle \nabla f_t(\mathbf{x}_t^*), \mathbf{x}_t - \mathbf{x}_t^* \rangle + \frac{L}{2} \|\mathbf{x}_t - \mathbf{x}_t^*\|^2 \right) \\ & \stackrel{(b)}{\leq} \frac{1}{2\xi} \sum_{t=1}^T \|\nabla f_t(\mathbf{x}_t^*)\|^2 + \frac{L + \xi}{2} \sum_{t=1}^T \|\mathbf{x}_t - \mathbf{x}_t^*\|^2 \\ & \stackrel{(c)}{\leq} \frac{1}{2\xi} \sum_{t=1}^T \|\nabla f_t(\mathbf{x}_t^*)\|^2 + \frac{L + \xi}{2} \left(\tau_r R^2 + \sum_{t=\tau_r+1}^T \|\mathbf{x}_t - \mathbf{x}_t^*\|^2 \right) \end{aligned} \quad (30)$$

where (a) follows from $f_t(\mathbf{x})$ being L -smooth in (11), (b) is because $\langle \mathbf{a}, \mathbf{b} \rangle \leq \frac{1}{2\xi} \|\mathbf{a}\|^2 + \frac{\xi}{2} \|\mathbf{b}\|^2$ for any $\xi > 0$, and (c) follows from the radius of \mathcal{X} being bounded in (13).

We now bound $\sum_{t=\tau_r+1}^T \|\mathbf{x}_t - \mathbf{x}_t^*\|^2$ in (30). We have

$$\begin{aligned} & \sum_{t=\tau_r+1}^T \|\mathbf{x}_t - \mathbf{x}_t^*\|^2 \\ & \stackrel{(a)}{\leq} \sum_{t=\tau_r+1}^T \left(\eta^{J_1} \|\hat{\mathbf{x}}_t^{J_1} - \mathbf{x}_t^*\|^2 \right) + \frac{1 - \eta^{J_1}}{1 - \eta} \beta \Delta_{2,T} \end{aligned} \quad (31)$$

where (a) follows from applying Lemma 2 to $\mathbf{P3}$ for J_1 times such that $\|\mathbf{x}_t - \mathbf{x}_t^*\|^2 \leq \eta^{J_1} \|\hat{\mathbf{x}}_t^{J_1} - \mathbf{x}_t^*\|^2 + \beta \sum_{i=1}^{J_1} \eta^{i-1} \|\nabla \hat{f}_t(\hat{\mathbf{x}}_t^{J_1-i}) - \nabla f_t(\hat{\mathbf{x}}_t^{J_1-i})\|^2$ for any $t > \tau_r$, and the definition of $\Delta_{2,T}$ in (7). We continue to bound $\sum_{t=\tau_r+1}^T \|\hat{\mathbf{x}}_t^{J_1} - \mathbf{x}_t^*\|^2$ in (31) as follows:

$$\sum_{t=\tau_r+1}^T \|\hat{\mathbf{x}}_t^{J_1} - \mathbf{x}_t^*\|^2$$

$$\begin{aligned} & \stackrel{(a)}{\leq} 2 \sum_{t=\tau_r+1}^T \left(\|\hat{\mathbf{x}}_t^{J_1} - \mathbf{x}_{t-\tau_r}^*\|^2 + \|\mathbf{x}_t^* - \mathbf{x}_{t-\tau_r}^*\|^2 \right) \\ & \stackrel{(b)}{\leq} 2 \sum_{t=\tau_r+1}^T \left(\|\hat{\mathbf{x}}_t^{J_1} - \mathbf{x}_{t-\tau_r}^*\|^2 \right) + 2\tau_r^2 \Pi_{2,T}^* \\ & \stackrel{(c)}{\leq} 2 \sum_{t=\tau_r+1}^T \left(\eta^{J_1} \|\mathbf{x}_{t-\tau_r} - \mathbf{x}_{t-\tau_r}^*\|^2 \right) + 2\tau_r^2 \Pi_{2,T}^* \\ & \quad + \frac{2(1 - \eta^{J_1})}{1 - \eta} \beta \Delta_{2,T} \end{aligned} \quad (32)$$

where (a) is because $\|\mathbf{a} + \mathbf{b}\|^2 \leq 2(\|\mathbf{a}\|^2 + \|\mathbf{b}\|^2)$, (b) follows from the definition of $\Pi_{2,T}^*$ in (5) and $|\sum_{i=1}^n x_i| \leq \sum_{i=1}^n |x_i| \leq \sqrt{n \sum_{i=1}^n |x_i|^2}$ such that $\|\mathbf{x}_t^* - \mathbf{x}_{t-\tau_r}^*\|^2 \leq \tau_r \sum_{i=1}^{\tau_r} \|\mathbf{x}_{t-\tau_r+i}^* - \mathbf{x}_{t-\tau_r+i-1}^*\|^2$, and (c) follows from applying Lemma 2 to $\mathbf{P2}$ for J_r times similar to (a) in (31).

Substituting (32) into (31), noting that $\sum_{t=\tau_r+1}^T \|\mathbf{x}_{t-\tau_r} - \mathbf{x}_{t-\tau_r}^*\|^2 \leq \sum_{t=1}^T \|\mathbf{x}_t - \mathbf{x}_t^*\|^2$, and rearranging terms, we have

$$\begin{aligned} & \left(1 - 2\eta^{J_1+J_r}\right) \sum_{t=\tau_r+1}^T \|\mathbf{x}_t - \mathbf{x}_t^*\|^2 - 2\eta^{J_1+J_r} \sum_{t=1}^{\tau_r} \|\mathbf{x}_t - \mathbf{x}_t^*\|^2 \\ & \leq 2\eta^{J_1} \tau_r^2 \Pi_{2,T}^* + \frac{2\eta^{J_1}(1 - \eta^{J_r}) + 1 - \eta^{J_1}}{1 - \eta} \beta \Delta_{2,T}. \end{aligned} \quad (33)$$

Substituting into (33) into (30), noting that $\eta < 1$ and the radius of \mathcal{X} being bounded in (13), and on the condition $2\eta^{J_1+J_r} < 1$, we complete the proof. ■

APPENDIX C PROOF OF THEOREM 5

Proof: We first prove claim i). We can show that (26) still holds by replacing τ_r with τ . Applying Lemma 2 to $\mathbf{P3}$ and $\mathbf{P2}$ for J_1 and J_r times, respectively, similar to the proofs of (27) and (28), we can show that

$$\begin{aligned} & \sum_{t=\tau+1}^T \|\mathbf{x}_t - \mathbf{x}_t^*\| \leq \tau \Pi_T^* + \sum_{t=\tau+1}^T \|\mathbf{x}_t - \mathbf{x}_{t-\tau}^*\| \\ & \leq \tau \Pi_T^* + \sqrt{\eta^{J_1}} \sum_{t=\tau+1}^T \left(\|\hat{\mathbf{x}}_t^{J_1} - \mathbf{x}_{t-\tau}^*\| \right) + \frac{1 - \sqrt{\eta^{J_1}}}{1 - \sqrt{\eta}} \sqrt{\beta} \Delta_T \\ & \leq \tau \Pi_T^* + \sqrt{\eta^{J_1}} \tau_r \Pi_T^* + \sqrt{\eta^{J_1+J_r}} \sum_{t=\tau+1}^T \left(\|\mathbf{x}_{t-\tau} - \mathbf{x}_{t-\tau}^*\| \right) \\ & \quad + \frac{\sqrt{\eta^{J_1}}(1 - \sqrt{\eta^{J_r}})}{1 - \sqrt{\eta}} \sqrt{\beta} \Delta_T + \frac{1 - \sqrt{\eta^{J_1}}}{1 - \sqrt{\eta}} \sqrt{\beta} \Delta_T. \end{aligned} \quad (34)$$

Rearranging terms of (34) and then substituting it into the version of (26) with τ_r replaced by τ , we prove claim i).

We now prove claim ii). We can show that (30) still holds by replacing τ_r with τ and

$$\begin{aligned} & \sum_{t=\tau+1}^T \|\mathbf{x}_t - \mathbf{x}_t^*\|^2 \leq 2 \sum_{t=\tau+1}^T \left(\|\mathbf{x}_t - \mathbf{x}_{t-\tau}^*\|^2 + \|\mathbf{x}_t^* - \mathbf{x}_{t-\tau}^*\|^2 \right) \\ & \leq 2\tau^2 \Pi_{2,T}^* + 2 \sum_{t=\tau+1}^T \|\mathbf{x}_t - \mathbf{x}_{t-\tau}^*\|^2. \end{aligned} \quad (35)$$

By applying Lemma 2 to **P3** and **P2** for J_1 and J_r times, respectively, similar to the proof of (32), we can show that

$$\begin{aligned}
& \sum_{t=\tau+1}^T \|\mathbf{x}_t - \mathbf{x}_{t-\tau}^*\|^2 \\
& \leq \eta^{J_1} \sum_{t=\tau+1}^T \left(\|\hat{\mathbf{x}}_t^{J_r} - \mathbf{x}_{t-\tau}^*\|^2 \right) + \frac{1-\eta^{J_1}}{1-\eta} \beta \Delta_{2,T} \\
& \leq 2\eta^{J_1} \sum_{t=\tau+1}^T \left(\|\hat{\mathbf{x}}_t^{J_r} - \mathbf{x}_{t-\tau}^*\|^2 \right) + 2\eta^{J_1} \tau_r^2 \Pi_{2,T}^* + \frac{1-\eta^{J_1}}{1-\eta} \beta \Delta_{2,T} \\
& \leq 2\eta^{J_1+J_r} \sum_{t=\tau+1}^T \left(\|\mathbf{x}_{t-\tau} - \mathbf{x}_{t-\tau}^*\|^2 \right) + 2\eta^{J_1} \frac{(1-\eta^{J_r})}{1-\eta} \beta \Delta_{2,T} \\
& \quad + 2\eta^{J_1} \tau_r^2 \Pi_{2,T}^* + \frac{1-\eta^{J_1}}{1-\eta} \beta \Delta_{2,T}. \tag{36}
\end{aligned}$$

Substituting (36) into (35) and rearranging terms, we have

$$\begin{aligned}
& (1-4\eta^{J_1+J_r}) \sum_{t=\tau+1}^T \|\mathbf{x}_t - \mathbf{x}_t^*\|^2 - 4\eta^{J_1+J_r} \sum_{t=1}^{\tau} \|\mathbf{x}_t - \mathbf{x}_t^*\|^2 \\
& \leq (2\tau_1^2 + 4\eta^{J_1} \tau_r^2) \Pi_{2,T}^* + \left(4\eta^{J_1} \frac{(1-\eta^{J_r})}{1-\eta} + 2 \frac{1-\eta^{J_1}}{1-\eta} \right) \beta \Delta_{2,T}.
\end{aligned}$$

Substituting the above inequality into the version of (30) with τ_r replaced by τ , noting that $\eta < 1$, and on condition that $4\eta^{J_1+J_r} < 1$, we complete the proof. ■

REFERENCES

- [1] S. Shalev-Shwartz, "Online learning and online convex optimization," *Found. Trends Mach. Learn.*, vol. 4, pp. 107–194, Feb. 2012.
- [2] M. Zinkevich, "Online convex programming and generalized infinitesimal gradient ascent," in *Proc. Intel. Conf. Mach. Learn. (ICML)*, 2003.
- [3] E. Hazan, A. Agarwal, and S. Kale, "Logarithmic regret algorithms for online convex optimization," *Mach. Learn.*, vol. 69, pp. 169–192, 2007.
- [4] J. Langford, A. J. Smola, and M. Zinkevich, "Slow learners are fast," in *Proc. Adv. Neural Info. Proc. Sys. (NIPS)*, 2009.
- [5] K. Quanrud and D. Khashabi, "Online learning with adversarial delays," in *Proc. Adv. Neural Info. Proc. Sys. (NIPS)*, 2015.
- [6] E. C. Hall and R. M. Willett, "Online convex optimization in dynamic environments," *IEEE J. Sel. Topics Signal Process.*, vol. 9, pp. 647–662, Jun. 2015.
- [7] A. Jadbabaie, A. Rakhlin, S. Shahrampour, and K. Sridharan, "Online optimization: Competing with dynamic comparators," in *Proc. Intel. Conf. Artif. Intell. Statist. (AISTATS)*, 2015.
- [8] A. Mokhtari, S. Shahrampour, A. Jadbabaie, and A. Ribeiro, "Online optimization in dynamic environments: Improved regret rates for strongly convex problems," in *Proc. IEEE Conf. Decision Control (CDC)*, 2016.
- [9] L. Zhang, T. Yang, J. Yi, J. Rong, and Z.-H. Zhou, "Improved dynamic regret for non-degenerate functions," in *Proc. Adv. Neural Info. Proc. Sys. (NIPS)*, 2017.
- [10] A. S. Bedi, P. Sarma, and K. Rajawat, "Tracking moving agents via inexact online gradient descent algorithm," *IEEE J. Sel. Topics Signal Process.*, vol. 12, pp. 202–217, 2018.
- [11] R. Dixit, A. S. Bedi, R. Tripathi, and K. Rajawat, "Online learning with inexact proximal online gradient descent algorithms," *IEEE Trans. Signal Process.*, vol. 67, pp. 1338–1352, 2019.
- [12] 3GPP TS38.300, "3rd Generation Partnership Project Technical Specification Group Radio Access Network; NR; NR and NG-RAN Overall Description; Stage 2 (Release 15)."
- [13] B. Liang, "Mobile edge computing," in *Key Technologies for 5G Wireless Systems*. V. W. S. Wong, R. Schober, D. W. K. Ng, and L.-C. Wang, Eds., Cambridge University Press, 2017.
- [14] S. Hosseini, A. Chapman, and M. Mesbahi, "Online distributed optimization via dual averaging," in *Proc. IEEE Conf. Decision Control (CDC)*, 2013.
- [15] F. Yan, S. Sundaram, S. V. N. Vishwanathan, and Y. Qi, "Distributed autonomous online learning: Regrets and intrinsic privacy-preserving properties," *IEEE Trans. Knowl. Data Eng.*, vol. 25, pp. 2483–2493, Nov. 2013.
- [16] A. Nedić, S. Lee, and M. Raginsky, "Decentralized online optimization with global objectives and local communication," in *Proc. Amer. Control Conf. (ACC)*, 2015.
- [17] K. I. Tsianos and M. G. Rabbat, "Efficient distributed online prediction and stochastic optimization with approximate distributed averaging," *IEEE Trans. Signal Inf. Process. Netw.*, vol. 2, pp. 489–506, Dec. 2016.
- [18] N. Ferdinand, H. Al-Lawati, S. Draper, and M. Nokleby, "Anytime minibatch: Exploiting stragglers in online distributed optimization," in *Proc. Intel. Conf. Learn. Rep. (ICLR)*, 2019.
- [19] D. Mateos-Nunez and J. Cortes, "Distributed online convex optimization over jointly connected digraphs," *IEEE Trans. Netw. Sci. Eng.*, vol. 1, pp. 23–37, Oct. 2014.
- [20] M. Akbari, B. Ghahesifard, and T. Linder, "Distributed online convex optimization on time-varying directed graphs," *IEEE Trans. Control Netw. Syst.*, vol. 4, pp. 417–428, Sep. 2017.
- [21] S. Shahrampour and A. Jadbabaie, "Distributed online optimization in dynamic environments using mirror descent," *IEEE Trans. Automat. Contr.*, vol. 63, pp. 714–725, Mar. 2018.
- [22] N. Eshraghi and B. Liang, "Distributed online optimization over a heterogeneous network with any-batch mirror descent," in *Proc. Intel. Conf. Mach. Learn. (ICML)*, 2020.
- [23] Y. Zhang, R. J. Ravier, M. M. Zavlanos, and V. Tarokh, "A distributed online convex optimization algorithm with improved dynamic regret," in *Proc. IEEE Conf. Decision Control (CDC)*, 2019.
- [24] M. Mahdavi, R. Jin, and T. Yang, "Trading regret for efficiency: Online convex optimization with long term constraints," *J. Mach. Learn. Res.*, vol. 13, pp. 2503–2528, Sep. 2012.
- [25] H. Yu, M. J. Neely, and X. Wei, "Online convex optimization with stochastic constraints," in *Proc. Adv. Neural Info. Proc. Sys. (NIPS)*, 2017.
- [26] T. Chen, Q. Ling, and G. B. Giannakis, "An online convex optimization approach to proactive network resource allocation," *IEEE Trans. Signal Process.*, vol. 65, pp. 6350–6364, Dec. 2017.
- [27] M. Abadi, A. Chu, I. Goodfellow, H. B. McMahan, I. Mironov, K. Talwar, and L. Zhang, "Deep learning with differential privacy," in *Proc. ACM SIGSAC Conf. Comput. Commun. Secur. (CCS)*, 2016.
- [28] O. Besbes, Y. Gur, and A. Zeevi, "Non-stationary stochastic optimization," *Oper. Res.*, vol. 63, pp. 1227–1244, Sep. 2015.
- [29] D. Gesbert, S. Hanly, H. Huang, S. Shamai Shitz, O. Simeone, and W. Yu, "Multi-cell MIMO cooperative networks: A new look at interference," *IEEE J. Sel. Topics Signal Process.*, vol. 28, pp. 1380–1408, Dec. 2010.
- [30] H. Zhang, N. B. Mehta, A. F. Molisch, J. Zhang, and S. H. Dai, "Asynchronous interference mitigation in cooperative base station systems," *IEEE Trans. Wireless Commun.*, vol. 7, pp. 155–165, Jan. 2008.
- [31] R. Zhang, "Cooperative multi-cell block diagonalization with per-base-station power constraints," *IEEE J. Sel. Areas Commun.*, vol. 28, pp. 1435–1445, Oct. 2010.
- [32] F. Amirnavaei and M. Dong, "Online power control optimization for wireless transmission with energy harvesting and storage," *IEEE Trans. Wireless Commun.*, vol. 15, pp. 4888–4901, Jul. 2016.
- [33] P. Mertikopoulos and E. V. Belmega, "Learning to be green: Robust energy efficiency maximization in dynamic MIMO-OFDM system," *IEEE J. Sel. Areas Commun.*, vol. 34, pp. 743–757, Apr. 2016.
- [34] H. Yu and M. J. Neely, "Dynamic transmit covariance design in MIMO fading systems with unknown channel distributions and inaccurate channel state information," *IEEE Trans. Wireless Commun.*, vol. 16, pp. 3996–4008, Jun. 2017.
- [35] J. Wang, M. Dong, B. Liang, and G. Boudreau, "Online downlink MIMO wireless network virtualization in fading environments," in *Proc. IEEE Global Commun. Conf. (GLOBECOM)*, 2019.
- [36] J. Wang, M. Dong, B. Liang, and G. Boudreau, "Online precoding design for downlink MIMO wireless network virtualization with imperfect CSI," in *Proc. IEEE Conf. Comput. Commun. (INFOCOM)*, 2020.
- [37] O. Somekh, O. Simeone, Y. Bar-Ness, A. M. Haimovich, and S. Shamai, "Cooperative multicell zero-forcing beamforming in cellular downlink channels," *IEEE Trans. Inf. Theory*, vol. 55, pp. 3206–3219, Jul. 2009.
- [38] H. Holma and A. Toskala, *WCDMA for UMTS - HSPA evolution and LTE*. John Wiley & Sons, 2010.
- [39] I. Abou-Faycal, M. Medard, and U. Madhow, "Binary adaptive coded pilot symbol assisted modulation over rayleigh fading channels without feedback," *IEEE Trans. Commun.*, vol. 53, pp. 1036–1046, Jun. 2005.